cmgh
CELLULAR AND MOLECULAR GASTROENTEROLOGY AND HEPATOLOGY

ORIGINAL RESEARCH

Oxaliplatin-Resistant Hepatocellular Carcinoma Drives Immune Evasion Through PD-L1 Up-Regulation and PMN-Singular Recruitment

Feng Zhang,[1,2,*] Keshu Hu,[1,2,*] Wenfeng Liu,[1,2] Bing Quan,[1,2] Miao Li,[1,2] Shenxin Lu,[1,2] Rongxin Chen,[1,2] Zhenggang Ren,[1,2] and Xin Yin[1,2]

[1]*Liver Cancer Institute, Zhongshan Hospital, Fudan University, Shanghai, China; and* [2]*National Clinical Research Center for Interventional Medicine, Zhongshan Hospital, Fudan University, Shanghai, China*

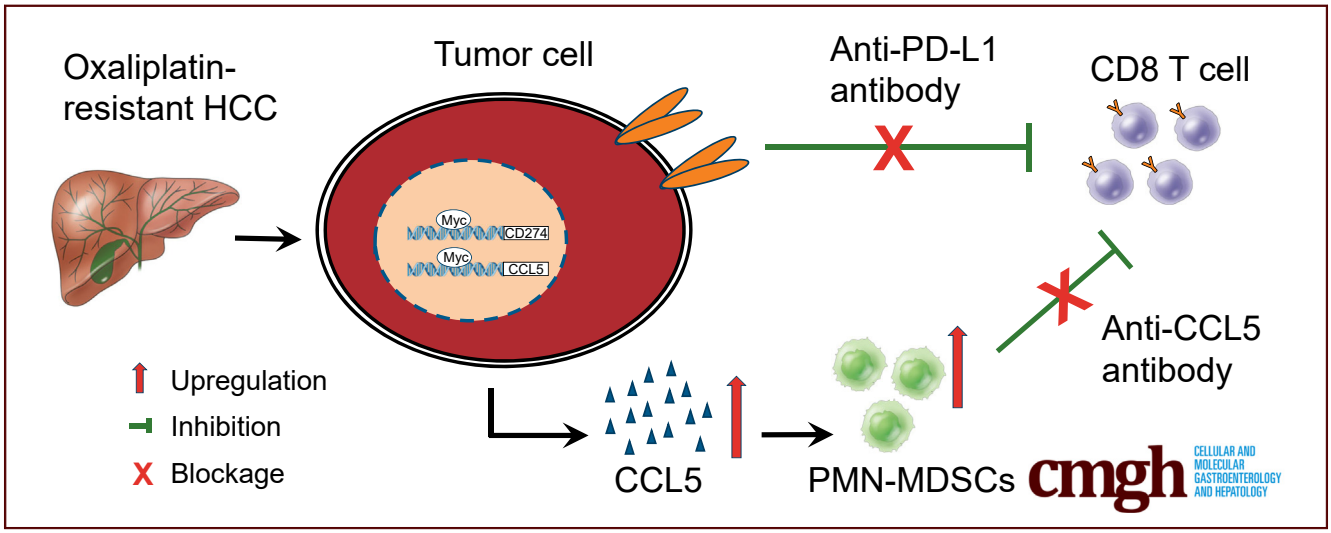

SUMMARY

This study dissects the mechanisms underlying the immune evasion of oxaliplatin-resistant hepatocellular carcinoma. The combination with programmed death-ligand 1 and CCL5 blockades could represent a promising antitumor strategy for oxaliplatin-resistance hepatocellular carcinoma.

BACKGROUND & AIMS: Previously, we showed the inhibitor of differentiation or DNA binding 1 (ID1)/Myc signaling is highly expressed in oxaliplatin-resistant hepatocellular carcinoma (HCC). This study sought to investigate the role of ID1/Myc signaling on immune evasion in oxaliplatin-resistant HCC.

METHODS: The oxaliplatin (OXA)-resistant HCC cell lines (Hepa 1-6–OXA, 97H-OXA, and 3B-OXA) were established and their oxaliplatin tolerance was confirmed in vitro and in vivo. The relationship between ID1/Myc and programmed death-ligand 1 (PD-L1) up-regulation and polymorphonuclear myeloid-derived suppressor cell (PMN-MDSC) accumulation was explored. The underlying mechanism in which ID1/Myc signaling regulated PD-L1 expression and PMN-MDSC accumulation was investigated in vitro and vivo.

RESULTS: Increased ID1/Myc expression was identified in oxaliplatin-resistant HCC and correlated with PD-L1 up-regulation and PMN-MDSC accumulation. The knockdown of Myc sensitized oxaliplatin-resistant HCC cells to oxaliplatin and resulted in a decrease of PMN-MDSCs and an increase of interferon-γ^+ $CD8^+$ T cells in a tumor microenvironment. Polymerase chain reaction array, enzyme-linked immunosorbent assay, and MDSC Transwell migration assay indicated that oxaliplatin-resistant HCC cells recruited PMN-MDSCs through chemokine (C-C motif) ligand 5 (CCL5). The dual luciferase reporter assay and chromatin immunoprecipitation assay indicated that Myc could directly increase the transcriptions of PD-L1 and CCL5. Furthermore, anti–PD-L1 antibody combined with CCL5 blockade showed significant antitumor effects in oxaliplatin-resistant HCC.

CONCLUSIONS: ID1/Myc signaling drives immune evasion in oxaliplatin-resistant HCC via PD-L1 up-regulation and PMN-MDSC recruitment. Blocking the ID1/Myc-induced immune tolerance represents a promising treatment target to conquer

chemoresistance in HCC. *(Cell Mol Gastroenterol Hepatol 2023;15:573–591; https://doi.org/10.1016/j.jcmgh.2022.12.002)*

Keywords: Hepatocellular Carcinoma; Chemoresistance; Immune Evasion; Immune Checkpoint; Polymorphonuclear Myeloid-Derived Suppressor Cell.

Hepatocellular carcinoma (HCC) is one of the most common malignant tumors worldwide and the third leading cause of cancer-related death. China alone accounts for approximately 55% of all new cases worldwide.[1,2] Notably, most HCC patients are already in the intermediate or advanced stage at diagnosis. For unresectable advanced HCC, systemic therapy and local regional therapies including platinum-based transcatheter arterial chemoembolization (TACE) and hepatic infusion chemotherapy are recommended.[3]

Oxaliplatin is a third-generation platinum analog that has been used in combination with 5-fluorouracil and leucovorin (FOLFOX4) as the standard chemotherapy regimen in advanced HCC.[4] As a DNA interacting agent, oxaliplatin covalently binds to DNA and forms intrastrand adducts to block DNA replication and transcription.[5] It also has been shown that oxaliplatin could regulate antitumor immune response and induce immunogenic cell death in HCC.[6] However, the existence of tumor intrinsic or acquired chemoresistance is a major limitation to the efficacy of platinum-based treatments. Current studies have suggested that oxaliplatin resistance is associated with drug efflux pumping, DNA damage repair, and epigenetic alternation.[7,8] Immune checkpoint inhibitors such as anti–programmed death 1 (PD-1)/programmed death-ligand 1 (PD-L1) antibodies were applied to treat HCC patients who failed to respond to chemotherapeutic drugs. However, the efficacy of PD-1/PD-L1 blockage monotherapy was modest with an overall objective response rate lower than 20%.[9] Therefore, it is urgent to explore the immunologic mechanisms underlying oxaliplatin resistance in HCC.

Immune evasion is one of the major hallmarks of HCC, the main mechanisms of which include the recruitment of immune-suppressive cells such as myeloid-derived suppressor cells (MDSCs), regulatory T cells (Tregs), tumor-associated macrophages, and activation of immune checkpoint signals such as the PD-1/PD-L1 axis.[10] MDSCs, a heterogeneous population of immature myeloid cells, are considered major regulators of immune responses in cancer and other pathologic conditions.[11] Based on their phenotypic and morphologic features, MDSCs are divided mainly into 2 subsets: granulocytic or polymorphonuclear MDSCs (PMN-MDSCs), and monocytic MDSCs (Mo-MDSCs). PMN-MDSCs and Mo-MDSCs have unique functional characteristics and play different roles in various pathologic conditions.[12] In the tumor microenvironment, MDSCs were able to suppress the proliferation and antitumor activities of T cells and natural killer cells through depleting lymphocyte nutrients (L-arginine, L-cysteine), producing oxidative stress (reactive oxygen species and reactive nitrogen species), and releasing anti-inflammation cytokines.[13] The essential role of MDSCs in the progression of HCC has been clarified in previous studies.[14] This study aims to investigate how MDSCs regulate oxaliplatin-resistance in HCC.

The inhibitor of differentiation or DNA binding 1 (ID1) is a member of the helix–loop–helix family, which is overexpressed in various types of cancer and generally is considered as an oncogene.[15] The Myc (also known as c-Myc) proto-oncogene codes for a transcription factor that coordinates the transcriptional expression of thousands of genes involved in the cell cycle, self-renewal, growth, differentiation, and metabolism.[16] In recent years, researchers have proposed that Myc also serves as a core regulator of antitumor immune response in tumor microenvironment.[17,18] In our previous study, we showed that ID1/Myc signaling conferred resistance to oxaliplatin in HCC through activating the pentose phosphate pathway.[19] Herein, we found ID1/Myc signaling drove immune evasion in oxaliplatin-resistant HCC via PD-L1 up-regulation and PMN-MDSC recruitment in the tumor microenvironment.

Results

The Characteristics of the Oxaliplatin-Resistant HCC

The oxaliplatin-resistant Hepa 1-6–oxaliplatin (OXA), 97H-OXA, and 3B-OXA cells were generated. The median inhibitory concentration (IC_{50}) was evaluated using the Cell Counting Kit-8 (CCK-8) assay. The IC_{50} of Hepa 1-6, 97H, and 3B cells was approximately 0.9 μmol/L, 0.25 μmol/L, and 0.25 μmol/L, respectively. In the oxaliplatin-resistant strains, the IC_{50} of Hepa 1-6–OXA, 97H-OXA, and 3B-OXA all increased to approximately 5 μmol/L (Figure 1*A*). Moreover, by using subcutaneous tumor models, we found that the tumor burden in the Hepa 1-6 group was decreased significantly after oxaliplatin treatment compared with the control group, whereas no statistical difference was observed in Hepa 1-6–OXA groups (Figure 1*B*). Our previous

***Authors share co-first authorship.**

Abbreviations used in this paper: **CCK-8, Cell Counting Kit-8; CCL5, chemokine (C-C motif) ligand 5; ChIP, chromatin immunoprecipitation; CM, conditioned media; CTLA-4, cytotoxic T-lymphocyte antigen 4; CXCL, chemokine (C-X-C motif) ligand; ELISA, enzyme-linked immunosorbent assay; Gr-1, myeloid-celll ineage differentiation antigen-1; HCC, hepatocellular carcinoma; IC_{50}, median inhibitory concentration; ID1, the inhibitor of differentiation or DNA binding 1; IFN, interferon; IP, intraperitoneally; MDSC, myeloid-derived suppressor cell; Mo, monocytic; mRNA, messenger RNA; MT, mutant; OS, overall survival; OXA, oxaliplatin; PD-1, programmed death 1; PD-L1, programmed death-ligand 1; PMN, polymorphonuclear; PSM, propensity score matching; qPCR, quantitative polymerase chain reaction; qRT-PCR, quantitative reverse-transcription polymerase chain reaction; shMyc, small hairpin RNA (shRNA) targeting Myc; shRNA, small hairpin RNA; TACE, transcatheter arterial chemoembolization; TCGA, The Cancer Genome Atlas; Treg, regulatory T cell; TUNEL, terminal deoxynucleotidyl transferase–mediated deoxyuridine triphosphate nick-end labeling; WT, wild-type.**

Most current article

2352-345X
https://doi.org/10.1016/j.jcmgh.2022.12.002

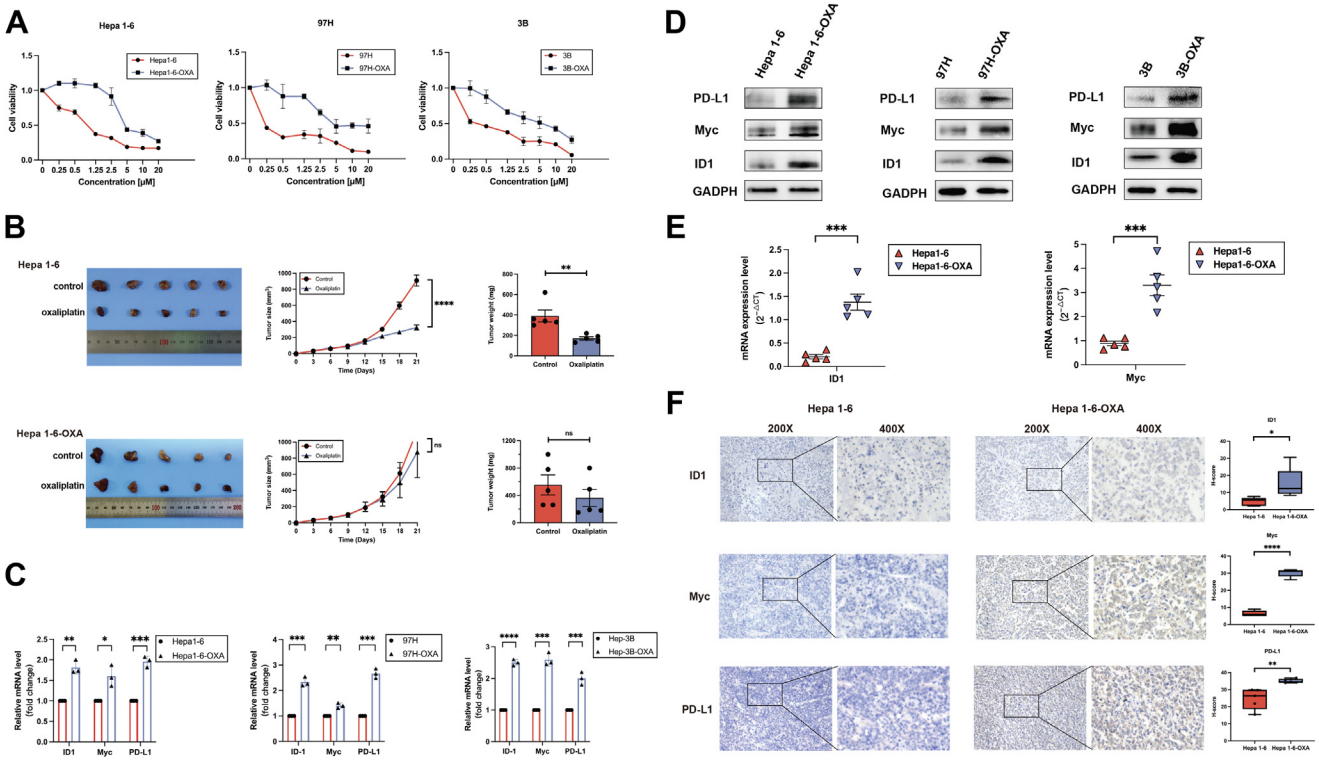

Figure 1. The characteristics of the oxaliplatin-resistant HCC. (*A*) Mouse (Hepa 1-6) and human (MHCC97H, Hep3B) HCC cell lines and their oxaliplatin-resistant cells (Hepa 1-6–OXA, 97H-OXA, and 3B-OXA) were treated with oxaliplatin at various concentrations for 72 hours. The IC_{50} values of Hepa 1-6–OXA, 97H-OXA, and Hep3B-OXA cells were significantly higher than those of their parent strain. (*B*) A total of 5×10^6 Hepa 1-6 cells and Hepa 1-6–OXA cells were inoculated into mice subcutaneously at the right flank. Mice were treated with oxaliplatin (10 mg/kg IP weekly) or vehicle ($n = 5$, each) when the tumor reached 50–100 mm^3. Tumor size was monitored with a caliper and tumor growth curves were plotted. Tumor weight was analyzed after death. (*C* and *D*) The overexpression of ID1, Myc, and PD-L1 in oxaliplatin-resistant HCC cells was shown by qRT-PCR and Western blot. (*E*) The increasing mRNA levels of ID1 and Myc in oxaliplatin-resistant tumors were determined by qRT-PCR. (*F*) Representative pictures and statistical diagrams of ID1, Myc, and PD-L1 immunohistochemical staining in Hepa 1-6 and Hepa 1-6–OXA tumor tissues are shown. GAPDH, glyceraldehyde-3-phosphate dehydrogenase. $^*P < .05$, $^{**}P < .01$, $^{***}P < .001$, and $^{****}P < .0001$.

study indicated that the ID1/Myc signaling endowed oxaliplatin resistance to HCC by activating the pentose phosphate pathway.[19] Next, we showed that ID1/Myc signaling was overexpressed in both human and mouse oxaliplatin-resistant HCC cells (Figure 1*C* and *D*). Moreover, quantitative reverse-transcription polymerase chain reaction (qRT-PCR) showed increased messenger RNA (mRNA) levels of both ID1 and Myc in oxaliplatin-resistant HCC tissues from tumor-bearing C57BL/6 mice (Figure 1*E*). Immunohistochemistry staining also confirmed that the expressions of ID1 and Myc were higher in oxaliplatin-resistant tumors compared with controls (Figure 1*F*). These data indicated that ID/Myc was overexpressed in oxaliplatin-resistant HCC both in vitro and in vivo.

Oxaliplatin-Resistant HCC Acquires Immune Privilege by ID1/Myc-Induced PD-L1 Up-Regulation

PD-L1 is selectively expressed on many tumors and plays a pivotal role in the ability of tumor cells to evade the host's immune system. Interestingly, in addition to overexpression of ID1/Myc signaling in the oxaliplatin-resistant HCC, the mRNA and protein levels of PD-L1 were up-regulated in human and mouse oxaliplatin-resistant HCC cells (Figure 1*C*–*F*). To investigate whether PD-L1 is regulated by ID1/Myc signaling, we established 2 Myc stable knockdown oxaliplatin-resistant strains for each cell line (Figure 2*A* and *B*). After the knockdown of Myc, the mRNA and protein expression of PD-L1 decreased in oxaliplatin-resistant HCC cells (Figure 2*A*–*C*). These results indicated that ID1/Myc signaling might involve PD-1/PD-L1–induced immune evasion in oxaliplatin-resistant HCC. Then, we sought to investigate whether oxaliplatin-resistant HCC cells could induce the dysfunction of effector T cells through PD-L1 up-regulation. The results of the T-cell–mediated tumor cell–killing assay showed that 97H-OXA and 3B-OXA cells were more resistant to activated T cells (Figure 2*D*) compared with their counterpart HCC cells. In addition, flow cytometric analysis showed that the percentages of granzyme$^+$CD8$^+$ T cells were decreased significantly after co-culture with oxaliplatin-resistant HCC (Figure 2*E* and *F*). Furthermore, we showed that the down-regulation of Myc sensitized oxaliplatin-resistant HCC cells to T-cell–mediated killing and restored the function of effector CD8$^+$ T cells (Figure 2*G*–*I*). These findings suggest that the activated

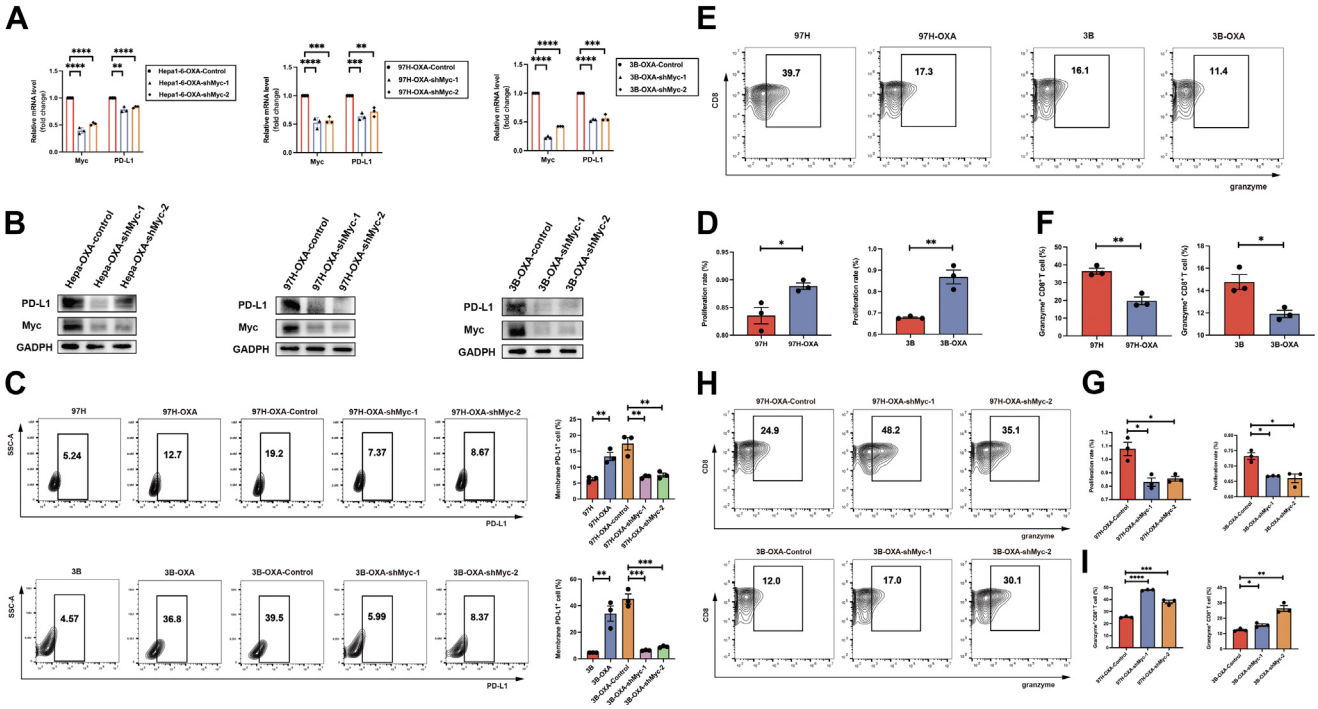

Figure 2. Oxaliplatin-resistant HCC acquires immune privilege by ID1/Myc-induced PD-L1 up-regulation. (*A* and *B*) Hepa 1-6–OXA, 97H-OXA, and 3B-OXA cells were transfected using lentiviral vectors with short hairpin RNA targeting the Myc gene. The up-regulation of PD-L1 upon Myc knockdown was confirmed by Western blot and qRT-PCR analyses. (*C*) The membrane expressions of PD-L1 were up-regulated in oxaliplatin-resistance cell lines (97H-OXA, 3B-OXA) and were down-regulated after Myc knockdown. (*D–I*) T-cell–mediated tumor-killing assay. The living HCC cells (*D*: 97H, 97H-OXA, 3B, 3B-OXA and *G*: 97H-OXA-control, 97H-OXA-shMyc-1/2, 3B-OXA-control, 3B-OXA-shMyc-1/2) were quantified by CCK-8. Flow cytometry analysis of the percentages of granzyme$^+$ CD8$^+$ T cells after co-culture with (*E* and *F*) oxaliplatin-resistant HCC cell lines and (*H* and *I*) Myc knockdown cell lines. The 2-tailed unpaired *t* test was used for analysis. **P* < .05, ***P* < .01, ****P* < .001, and *****P* < .0001. GAPDH, glyceraldehyde-3-phosphate dehydrogenase; SSC-A, side scatter-area.

ID1-Myc signaling up-regulated PD-L1 expression in oxaliplatin-resistant HCC and rendered the cells more resistant to activated T cells.

Immune Tolerance Tumor Microenvironment Is Remodeled by Oxaliplatin-Resistant HCC

To further explore the role of oxaliplatin-resistant HCC on the tumor immune microenvironment, we established HCC-bearing models in immune-competent mice (C57BL/6) by using Hepa 1-6 and Hepa 1-6–OXA cells. After treatments with 0.1 mL oxaliplatin (10 mg/kg/wk) for 3 weeks, the flow cytometric analysis showed that oxaliplatin-resistant tumors had increased infiltration of PMN-MDSCs (CD11b$^+$Ly6G$^+$) and Tregs (CD25$^+$FoxP3$^+$), while there was no significant difference in the frequency of Mo-MDSCs (CD11b$^+$Ly6C^{hi}) and tumor-associated macrophages (CD11b$^+$F4/80$^+$) (Figure 3*A–C*). Furthermore, the increased infiltration of MDSCs also was identified in the spleens of Hepa 1-6–OXA tumor-bearing mice compared with those with parent strain tumors (Figure 3*D*). In addition, oxaliplatin-resistant tumors had a decreased infiltration of CD8$^+$ T cells, which also showed an exhausted state, expressing higher levels of inhibitory receptors including cytotoxic T-lymphocyte antigen 4 (CTLA4) and T cell immunoglobulin domain and mucin domain-3 (Tim3), but lower levels of activation markers such as granzyme and perforin (Figure 3*E* and *F*).

As reported in previous studies, MDSCs are a heterogeneous population of cells with immunosuppressive activity, and can stimulate the expansion of Tregs and indirectly inhibit the function of effector T cells.[11] Therefore, we next confirmed the immunosuppressive function of PMN-MDSCs in vitro. The PMN-MDSCs were isolated from the spleen of mice. Then, we co-cultured PMN-MDSCs with splenic CD8$^+$ T cells at various ratios (1:1, 2:1, and 4:1). PMN-MDSCs showed dose-dependent immune suppression of CD8$^+$ T-cell proliferation (Figure 3*G*). All of these results suggest that oxaliplatin-resistant HCC may remodel immune tolerance tumor microenvironment through PMN-MDSCs recruitment.

ID1/Myc Signaling Drives PMN-MDSC Recruitment and Facilitates Oxaliplatin-Resistant HCC Progression

We subcutaneously inoculated the Hepa 1-6–OXA–control and Hepa 1-6–OXA–small hairpin RNA (shRNA) targeting Myc (shMyc) cells into C57BL/6 mice to develop HCC-bearing mouse models. After oxaliplatin

treatments, the growth rates and tumor weight in the Hepa 1-6–OXA–control group were significantly higher than those in the Hepa 1-6–OXA–shMyc group, indicating that Myc knockdown enhanced the therapeutic effects of oxaliplatin in vivo (Figure 4*A*). Based on the increasing evidence that Myc could regulate the tumor microenvironment through effects on immune effector cells and immune checkpoint moleculars,[17] we speculated that Myc

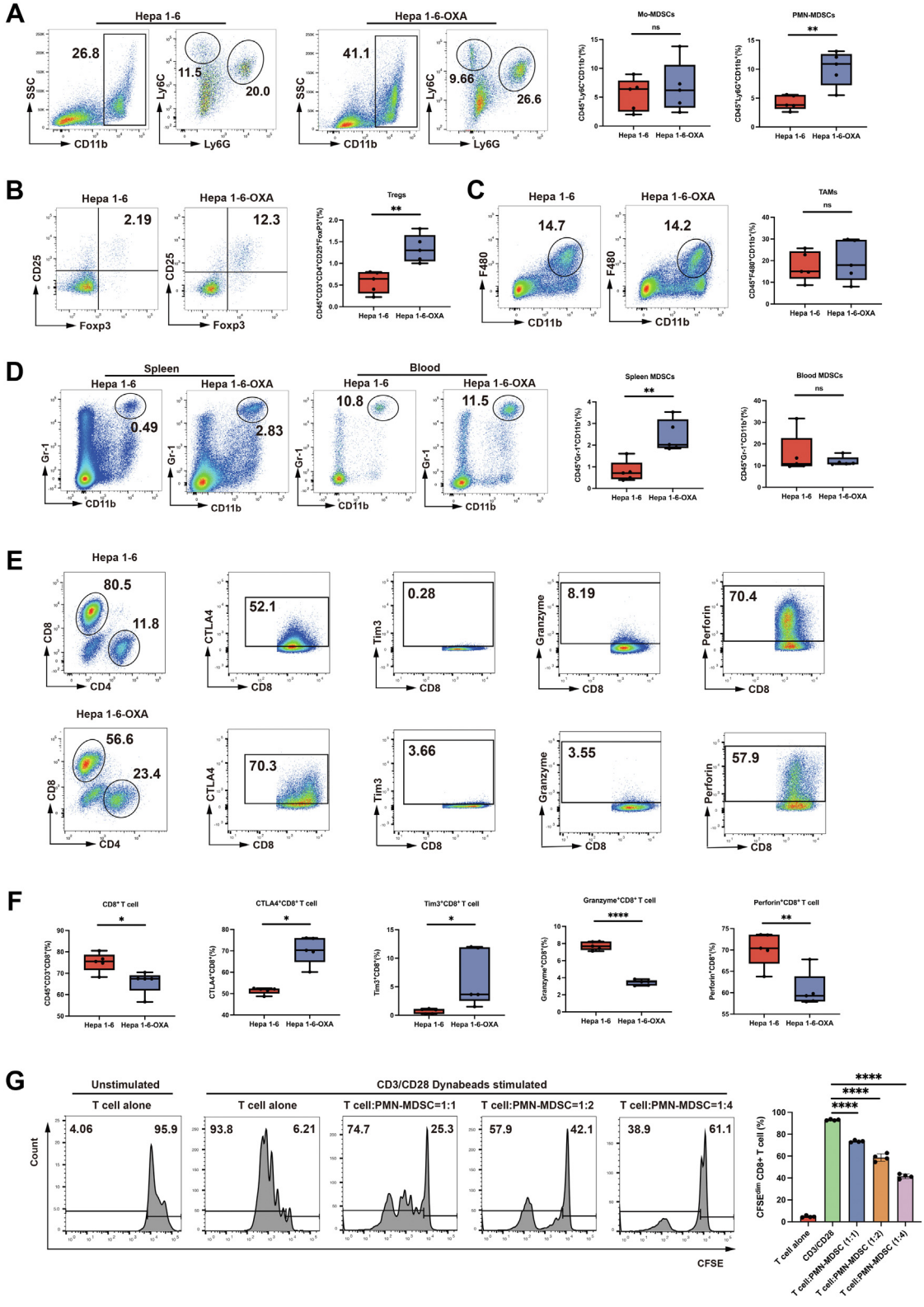

might be responsible for PMN-MDSC recruitment in oxaliplatin-resistant HCC. The flow cytometric analysis confirmed that knockdown of Myc in oxaliplatin-resistant HCC cells reduced the number of PMN-MDSCs in the tumor microenvironment (Figure 4*B*), but increased the number of $CD8^+$ T cells (Figure 4*C*). Moreover, the percentage of interferon (IFN)-γ^+CD8^+ T cells also was increased in Hepa 1-6–OXA–shMyc tumors, suggesting that Myc deficiency dampened PMN-MDSC infiltration and promoted IFN-γ^+CD8^+ T-cell–mediated antitumor immunity in oxaliplatin-resistant HCC (Figure 4*C*). Furthermore, immunohistochemistry staining also confirmed that Hepa 1-6–OXA–shMyc tumors presented with lower PD-L1 expression, decreased infiltration of $CD11b^+$ myeloid cells, and increased $CD8^+$ T cells, which was consistent with previous results (Figure 4*D* and *E*). The Ki67 immunostaining indicated that Hepa 1-6–OXA–shMyc tumors had a remarkable decrease in the positive cell rate compared with the controls, and the terminal deoxynucleotidyl transferase–mediated deoxyuridine triphosphate nick-end labeling (TUNEL) assay showed a significant increase in the positive cell rate in the Hepa 1-6–OXA–shMyc group (Figure 4*D* and *E*).

The mechanisms of PMN-MDSC accumulation in the tumor microenvironment may result from myeloid cell conversion or direct recruitment of PMN-MDSCs from immune organs and peripheral blood. Therefore, we first co-cultured mouse bone marrow–derived cells with conditioned media (CM) from Hepa 1-6 or Hepa 1-6–OXA cells for 4 days. Flow cytometry analysis indicated that oxaliplatin-resistant Hepa 1-6 cells did not affect the conversion of myeloid cells toward MDSCs (Figure 4*F*). Then, we performed a chemotaxis assay by using a co-culture system with Transwell membranes. The CM generated from Hepa 1-6 and Hepa 1-6–OXA was placed in the bottom wells of the Transwell inserts as chemoattractants. The splenic PMN-MDSCs from C57BL/6 mice were seeded in the upper chambers. Chemotaxis assays showed that the migration index of PMN-MDSCs was increased significantly after co-culture with CM from Hepa 1-6–OXA cells (Figure 4*G*). Moreover, in vitro Transwell assay also showed that Myc knockdown attenuated Hepa 1-6–OXA–CM–induced PMN-MDSC chemotaxis (Figure 4*H*).

To investigate whether Myc-induced PMN-MDSC recruitment promoted HCC progression, we adoptively transferred HCC cells and isolated splenic PMN-MDSCs into murine subcutis at a 5:1 ratio: (1) Hepa 1-6–OXA–control; (2) Hepa 1-6–OXA–shMyc; (3) Hepa 1-6–OXA–control and PMN-MDSCs; and (4) Hepa 1-6–OXA–shMyc and PMN-MDSCs. The results showed that the tumor growth rates and tumor weights in mice bearing Hepa 1-6–OXA–control cells combined with PMN-MDSCs were significantly higher in comparison with mice bearing Hepa 1-6–OXA–control cells. In addition, co-injection of Myc knockdown Hepa 1-6–OXA–shMyc cells and PMN-MDSCs also promoted the growth rates and tumor weights of HCC (Figure 4*I*). Taken together, these data supported the hypothesis that the ID1/Myc-mediated PMN-MDSC recruitment promoted oxaliplatin-resistant HCC progression.

Chemokine (C-C Motif) Ligand 5 Is the Key Mediator of ID1/Myc-Induced PMN-MDSC Recruitment

The MDSC migration assay showed that CM from Hepa 1-6–OXA cells possesses a stronger chemotactic ability for PMN-MDSCs, which was attenuated by Myc knockdown. To uncover the key factor of Myc-induced PMN-MDSCs recruitment, we applied a qRT-PCR array to quantify the expression of a panel of chemokines and cytokines in oxaliplatin-resistant Hepa 1-6–OXA cells. Of all the factors evaluated, CCL5 was one of the most significantly changed chemokines compared with any others regulated by Myc (Figure 5*A* lists the top 10). Indeed, the positive correlation between Myc and CCL5 was shown in a Gene Expression Omnibus data set (GSE14520) (Figure 5*B*). In addition, by using qRT-PCR and enzyme-linked immunosorbent assay (ELISA), we confirmed the fact that CCL5 was induced in oxaliplatin-resistant HCC and regulated by Myc (Figure 5*C*–*E*).

Previous studies have shown that chemokine (C-C motif) receptor 5^+ MDSCs show a stronger suppressive activity and tumor-derived CCL5 plays a pivotal role in chemokine (C-C motif) receptor 5-dependent mobilization of PMN-MDSCs, supporting our earlier-mentioned findings.[20] Furthermore, we investigated the chemotactic ability of CCL5 for PMN-MDSCs in oxaliplatin-resistant HCC by chemotaxis assay. We found that the chemotactic ability of CM generated from Hepa 1-6–OXA–control cells was drastically deprived by treatment with CCL5 neutralizing antibody, whereas no significant difference was observed between Hepa 1-6–OXA–shMyc group and Hepa

Figure 3. (***See previous page***). **Oxaliplatin-resistant HCC showed immune-tolerant tumor microenvironment.** (*A*–*C*) Hepa 1-6 and Hepa 1-6–OXA cells were inoculated into C57BL/6 mice and the infiltration of immune cells in Hepa 1-6 and Hepa 1-6–OXA tumors was analyzed by flow cytometry (n = 5 each). Higher numbers of $CD11b^+Ly6G^+$ PMN-MDSCs and $CD3^+CD4^+CD25^+FoxP3^+$ Tregs were infiltrated in Hepa 1-6–OXA tumors than in Hepa 1-6 tumors. Conversely, no significant difference was observed in the percentages of $CD11b^+Ly6C^+$ Mo-MDSCs and $CD11b^+F480^+$ tumor-associated macrophages (TAMs). (*D*) The expansion of $CD11b^+Gr\text{-}1^+$ MDSCs in the spleen and blood of mice with Hepa 1-6 or Hepa 1-6–OXA tumor was analyzed by flow cytometry (n = 5 each). $CD11b^+Gr\text{-}1^+$ MDSCs were pooled more frequently in the spleens of Hepa 1-6–OXA–bearing mice than that of Hepa 1-6–bearing mice, although no significant difference was observed in blood samples from Hepa 1-6 or Hepa 1-6–OXA–bearing mice. (*E* and *F*) Hepa 1-6–OXA tumors had reduced numbers of $CD3^+CD8^+$ T cells, which expressed higher levels of CTLA4 and T cell immunoglobulin domain and mucin domain-3 (Tim3), but lower levels of granzyme and perforin. (*G*) T-cell proliferation assay. The percentage of 5(6)-carboxyfluorescein succinimidyl ester (CFSE) low population represents the frequencies of proliferating $CD3^+CD8^+$ T cells. Representative flow cytometry data and a statistical diagram are shown. $^*P < .05$, $^{**}P < .01$, and $^{****}P < .0001$. SSC, side scatter.

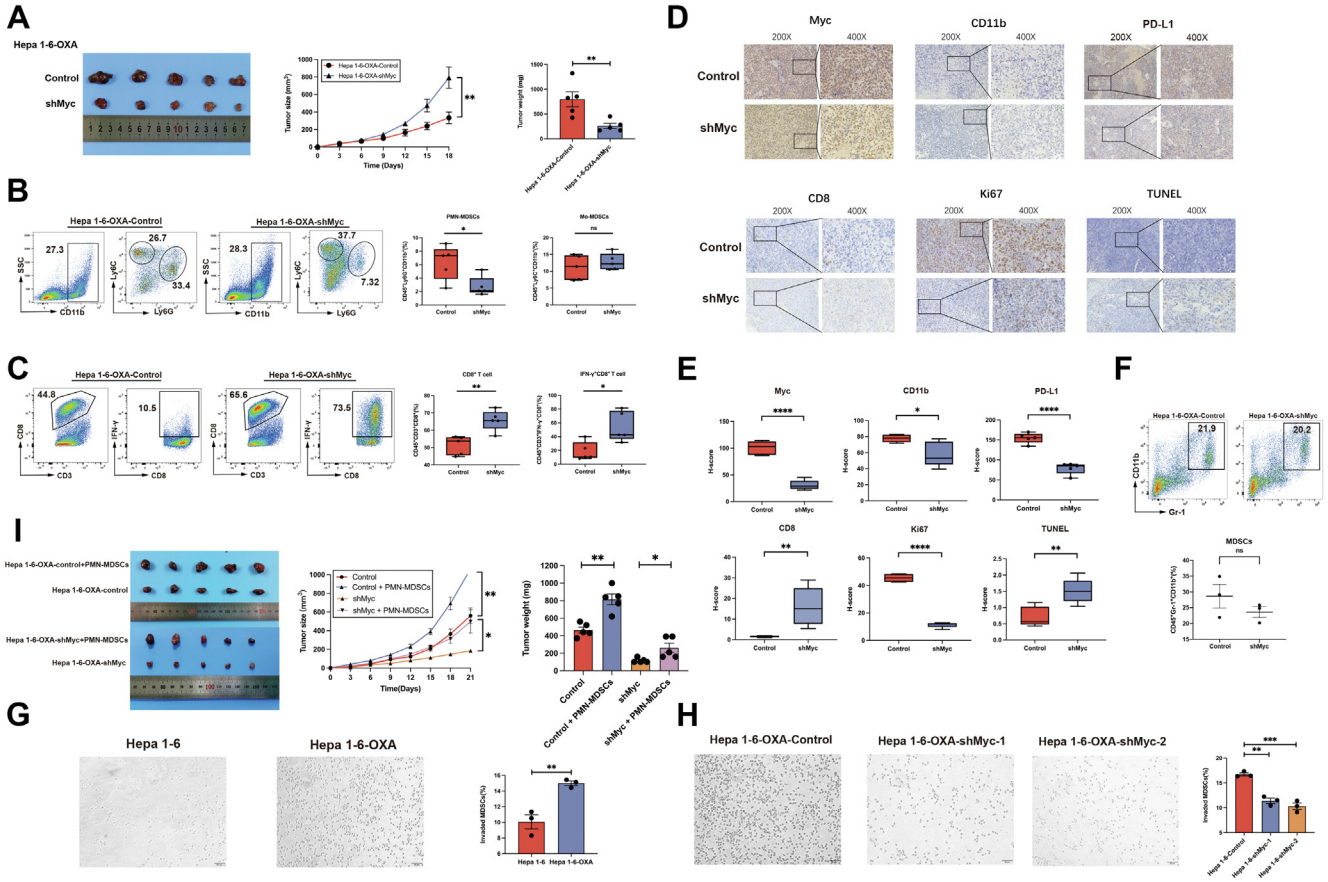

Figure 4. ID1/Myc signaling induces PMN-MDSC recruitment and promotes oxaliplatin-resistant HCC progression. (*A*) The Hepa 1-6–OXA–control and Hepa 1–6–OXA–shMyc–bearing mice were treated with oxaliplatin for 3 weeks (10 mg/kg IP weekly). The Hepa 1-6–OXA–control group showed a significantly higher tumor growth rate and tumor weight. (*B* and *C*) The harvested tumors were dissociated and the percentages of MDSCs and IFN-γ^+CD8$^+$ T cells were evaluated by flow cytometry. The representative CD11b$^+$Ly6G$^+$ PMN-MDSCs were decreased significantly and the frequency of CD3$^+$CD8$^+$ T cells and IFN-γ^+CD8$^+$ T cells was higher in the Hepa 1-6–OXA–shMyc group. (*D* and *E*) Representative pictures and statistical diagrams of Myc, CD11b, PD-L1, CD8, Ki67, and TUNEL immunohistochemical staining in Hepa 1-6–OXA–control and Hepa 1-6–OXA–shMyc tumor tissues are shown. (*F*) The influences of Hepa 1-6–OXA on the conversion of MDSCs. The isolated bone marrow–derived cells were co-cultured with CM from Hepa 1-6 or Hepa 1-6–OXA cells for 4 days. The flow cytometry analysis was applied to evaluate the percentages of transformed MDSCs (n = 3; $P = .2906$). (*G* and *H*) MDSC migration assays were performed by placing CM collected from Hepa 1-6, Hepa 1-6–OXA, Hepa 1-6–OXA–control, and Hepa 1-6–OXA–shMyc-1/2 in the lower chambers. Freshly isolated splenic PMN-MDSCs were seeded in the upper chambers and incubated for 36 hours. The total number of migrated MDSCs in the lower chambers was counted. (*I*) Hepa 1-6–OXA cells and PMN-MDSCs co-inoculation experiment. 5×10^6 Hepa 1-6–OXA cells alone, or 5×10^6 Hepa 1-6–OXA and 1×10^6 PMN-MDSCs were co-injected subcutaneously into C57BL/6 mice (n = 5 for each group). Tumor size was monitored with a caliper and tumor growth curves were plotted. Tumor weight was analyzed after death. *$P < .05$, **$P < .01$, ***$P < .001$, and ****$P < .0001$. SSC, side scatter.

1-6–OXA–shMyc treated with anti-CCL5 antibody group (Figure 5*F*).

Myc Enhances Transcriptional Activation of CCL5 and PD-L1

Our previous data showed that Myc was responsible for the increased levels of CCL5 and PD-L1 in oxaliplatin-resistant HCC. Moreover, in vivo data also confirmed the lower mRNA levels of CCL5 and PD-L1 in Hepa 1-6–OXA–shMyc tumors compared with Hepa 1-6–OXA–control tumors in vivo (Figure 6*A*). Myc is an important transcription factor that can regulate its downstream genes through direct activation or inhibition of gene transcription,[17] therefore, we considered the possibility of direct control of CCL5 and PD-L1 gene transcriptions by Myc. We first investigated whether Myc could bind to the CCL5 and PD-L1 promoters and predicted the possible transcription factor-binding sites by using Jaspar (http://Jaspar.genereg.net) and PROMO (http://alggen.lsi.upc.es) databases (Figure 6*B*). Then, the luciferase reporter assay was used to confirm this hypothesis. Myc expression plasmids were co-transfected with a wild-type CCL5 (-2000/+55)/Luc promoter construct (wild type [WT]) or a mutant CCL5 (-2000/+55)/Luc promoter construct with predicted potential binding sites mutated (MT) (Figure 6*C*). We observed that Myc overexpression stimulated WT CCL5 (-2000/+55)/Luc reporter gene activity, but failed to

enhance the MT CCL5 (-2000/+55)/Luc promoter activity (Figure 6*D*). This result indicated that Myc could bind directly to the CCL5 promoter and increase the transcription of CCL5. Similarly, to further address whether Myc regulates PD-L1 expression via direct transcriptional activation, we co-transfected a PD-L1 (-1942/+94)/Luc promoter construct and Myc expression plasmids into human embryonic kidney-293 cells. As shown in Figure 6*E*, Myc significantly enhanced PD-L1 promoter activity as well. In addition, using chromatin immunoprecipitation (ChIP)–quantitative polymerase chain reaction (qPCR) assay, we verified that Myc bound to predicted potential binding sites of the promoter regions of CCL5 and PD-L1 in both 97H and 97H-OXA cells (Figure 6*F* and *G*).

Blocking MDSC Exerts Antitumor Effects in Oxaliplatin-Resistant HCC

We have to date confirmed that ID1/Myc signaling induces PMN-MDSC recruitment and suppresses $CD8^+$ T-cell–mediated antitumor immunity, thus promoting tumor progression in oxaliplatin-resistant HCC. Then, to analyze the therapeutic effects of MDSC blockage in oxaliplatin-resistant HCC, we established the HCC-bearing mouse model by using Hepa 1-6–OXA–control and Hepa 1-6–OXA–shMyc cell lines. Our results showed that the anti–myeloid-celll ineage differentiation antigen-1 (Gr-1) antibody could inhibit tumor growth in both the Hepa 1-6–OXA–control and Hepa 1-6–OXA–shMyc groups (Figure 7*A*). The flow cytometric analysis showed that the anti–Gr-1 antibody could effectively decrease the PMN-MDSC infiltrations and increase the frequencies of $CD8^+$ T cells (Figure 7*B* and *C*). We further blocked MDSC chemotaxis in oxaliplatin-resistant HCC by using an anti-CCL5 antibody. The results showed that the anti-CCL5 antibody could significantly suppress the tumor growth in the Hepa 1-6–OXA–control group but not in Hepa 1-6–OXA–shMyc–bearing mice (Figure 7*D*). We also found that anti-CCL5 antibody could significantly decrease the frequencies of PMN-MDSCs in the Hepa 1-6–OXA–control group, but did not affect Mo-MDSC infiltration. Moreover, the anti-CCL5 antibody significantly increased the percentages of $CD8^+$ T cells in Hepa 1-6–OXA–control–bearing mice (Figure 7*E* and *F*). These findings indicated that the blockage of CCL5-induced PMN-MDSC chemotaxis could reverse immunosuppression and promote antitumor immunity in oxaliplatin-resistant HCC.

CCL5 Blockade Enhances the Antitumor Effect of Anti–PD-L1 Treatment in Oxaliplatin-Resistant HCC

We have shown that blocking PMN-MDSC infiltration by anti-CCL5 antibody reduced the tumor burden of oxaliplatin-resistant HCC, and oxaliplatin-resistant HCC also up-regulated PD-L1 expression to directly impair the function of cytotoxic T cell. Therefore, we next investigated the possibility that PD-L1 blockage might synergize with anti-CCL5 antibody to augment the antitumor immune response by using subcutaneous and orthotopic tumor xenograft models. In the subcutaneous tumor models, mice inoculated with Hepa 1-6–OXA cells were treated with anti–PD-L1 or combined with anti-CCL5 antibodies every 3 days and the effects of single or combined treatment on tumor growth were evaluated on day 18 (Figure 8*A*). Although anti–PD-L1 antibody alone could inhibit the progression of oxaliplatin-resistant HCC, the antitumor effect was more dramatic in the mice treated with both antibodies (Figure 8*B*). The flow cytometry analysis showed that the combination of anti–PD-L1 and anti-CCL5 treatments could significantly reduce the infiltration of PMN-MDSCs, and up-regulated the frequency of $CD8^+$ T cells (Figure 8*C* and *D*). In addition, compared with the isotype control and anti–PD-L1 alone, tumor-infiltrating $CD8^+$ T cells of the mice treated with combined anti–PD-L1 and anti-CCL5 antibodies showed significantly higher production of granzyme and perforin, as well as lower expression of exhausted marker CTLA4 (Figure 8*D*). Furthermore, using orthotopic tumor xenograft models, we showed that tumor weights in the group treated with both anti–PD-L1 and anti-CCL5 antibodies were the lowest (Figure 8*E*). Blocking CCL5 could significantly reduce PMN-MDSC infiltration in oxaliplatin-resistant tumors (Figure 8*F* and *G*). A combination of anti–PD-L1 and anti-CCL5 treatments induced the highest frequencies of $CD8^+$ T cells and $granzyme^+$ $perforin^+$ $CD8^+$ T cells (Figure 8*H* and *I*). We did not observe changes in body weights or significant side effects in these mice (Figure 8*J*).

The Overexpression of Myc Correlates With High Levels of PD-L1, MDSC Makers in HCC, and Indicates Poor Responses to Adjuvant TACE

Next, we sought to validate the relationships between Myc, PD-L1, and MDSC markers by using gene expression data from public data sets. The results showed that Myc was correlated positively with PD-L1 and MDSC markers (CD11b, CD33) in both The Cancer Genome Atlas (TCGA) and GEO (GSE14520) data sets (Figure 9*A* and *B*). Moreover, Kaplan–Meier analysis indicated that patients with higher expression levels of Myc, CD11b, and CD33 had significantly shorter overall survival rates in the TCGA data set (Figure 9*C*). Then, we validated these results in 352 paired human HCC tissues from our hospital (Zhongshan cohort) by immunohistochemistry (Figure 9*D*). Consistently, it has been observed that the expression level of Myc was correlated positively with PD-L1 and myeloid cell marker CD11b (Fig. 9*E*). Moreover, it has been shown that HCC patients with high infiltrations of $CD11b^+$ myeloid cells had significantly shorter overall survival (OS) and recurrence-free surviva (RFS) (Figure 9*F*). The outcome of HCC patients after postoperative adjuvant TACE was widely regarded as an indicator of chemosensitivity.[21,22] Next, we performed a propensity score matching (PSM) analysis to show the correlation between expression of Myc and responses to postoperative TACE in this cohort of 352 HCC patients receiving curative resection. Before PSM, the 1-, 2-, and 3-year OS rates in the non-TACE group were significantly higher than those in the TACE group: 88.5%, 80.2%, and 71.2% vs 75.3%, 57.4%, and 51.0%, respectively; $P < .001$)

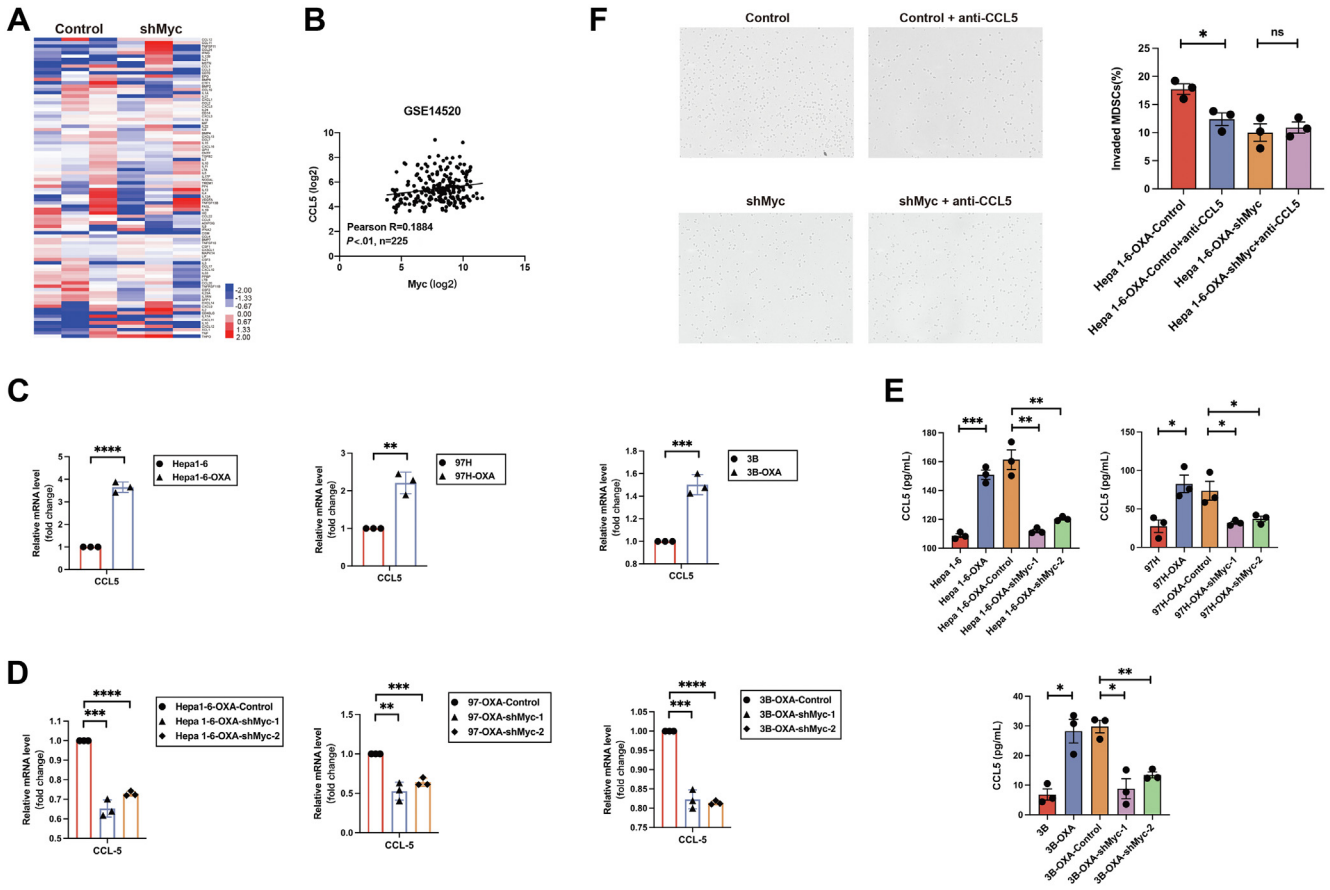

Figure 5. ID1/Myc induced PMN-MDSC recruitment through CCL5. (*A*) qRT-PCR array was performed for screening Myc-regulated chemokines responsible for PMN-MDSC recruitment. CCL5 was one of the top 10 most significantly changed chemokines. (*B*) Correlation analysis between Myc and CCL5 by using a cohort of 225 HCC patients (GSE14520). (*C–E*) The overexpression of CCL5 in oxaliplatin-resistant HCC cell lines and the down-regulation of CCL5 in Myc knockdown oxaliplatin-resistant HCC cell lines were confirmed by (*C* and *D*) qRT-PCR and (*E*) ELISA. (*F*) MDSC migration assays using CM from Hepa 1-6–control added by anti-CCL5 antibody or phosphate-buffered saline, or CM from Hepa 1-6–shMyc added by anti-CCL5 antibody or phosphate-buffered saline. *$P < .05$, **$P < .01$, ***$P < .001$, and ****$P < .0001$.

(Figure 9*G*). Considering that the distribution of clinical characteristics differed between the non-TACE and TACE groups, we performed PSM analysis and matched 46 pairs of non-TACE and TACE patients to reduce confounding factors and to reflect the true effects of postoperative TACE. All variables were balanced between the 2 groups (all $P > .2$) (Table 1). After PSM, the OS rates were comparable between the 2 groups ($P = .484$) (Figure 9*G*). Next, we divided these patients into Myc-low (N = 52) and Myc-high (N = 46) groups based on the median expression level of Myc. It is interesting that postoperative adjuvant TACE could provide a significant survival improvement in Myc-low patients but not Myc-high patients (Figure 9*H*). All of these results indicate that Myc serves as an important factor mediating responses of HCC patients to chemotherapeutic drugs.

Discussion

Platinum-based TACE and hepatic infusion chemotherapy have been the backbone of treatment in patients with unresectable advanced HCC in recent years. However, the efficacy of chemotherapy is limited for HCC patients with intrinsic or acquired drug resistance, which eventually results in treatment failure.[23] Although immunogenic cell death has been considered as an important step for chemotherapy in HCC,[6] the immunologic mechanisms underlying chemoresistance for oxaliplatin have not been elucidated in detail. In this study, we found that ID1/Myc signaling activation promoted oxaliplatin-resistant HCC immune evasion and tumor progression via PD-L1 up-regulation and CCL5-induced PMN-MDSC recruitment in HCC cells.

Previous studies have reported that overexpressed ID1 contributed to the development of HCC in patients with cirrhosis,[24] and correlated with HCC invasion and metastasis.[25] In recent years, the role of ID1 in the development of drug resistance has been explored further. Li et al[26] found that knockdown of ID1 in gastric cancer increased sensitivity to cisplatin. Przybyla et al[27] suggested that suppression of ID1 sensitized colon cancer cells to 5-fluorouracil. In our previous study, we found that ID1 was overexpressed in

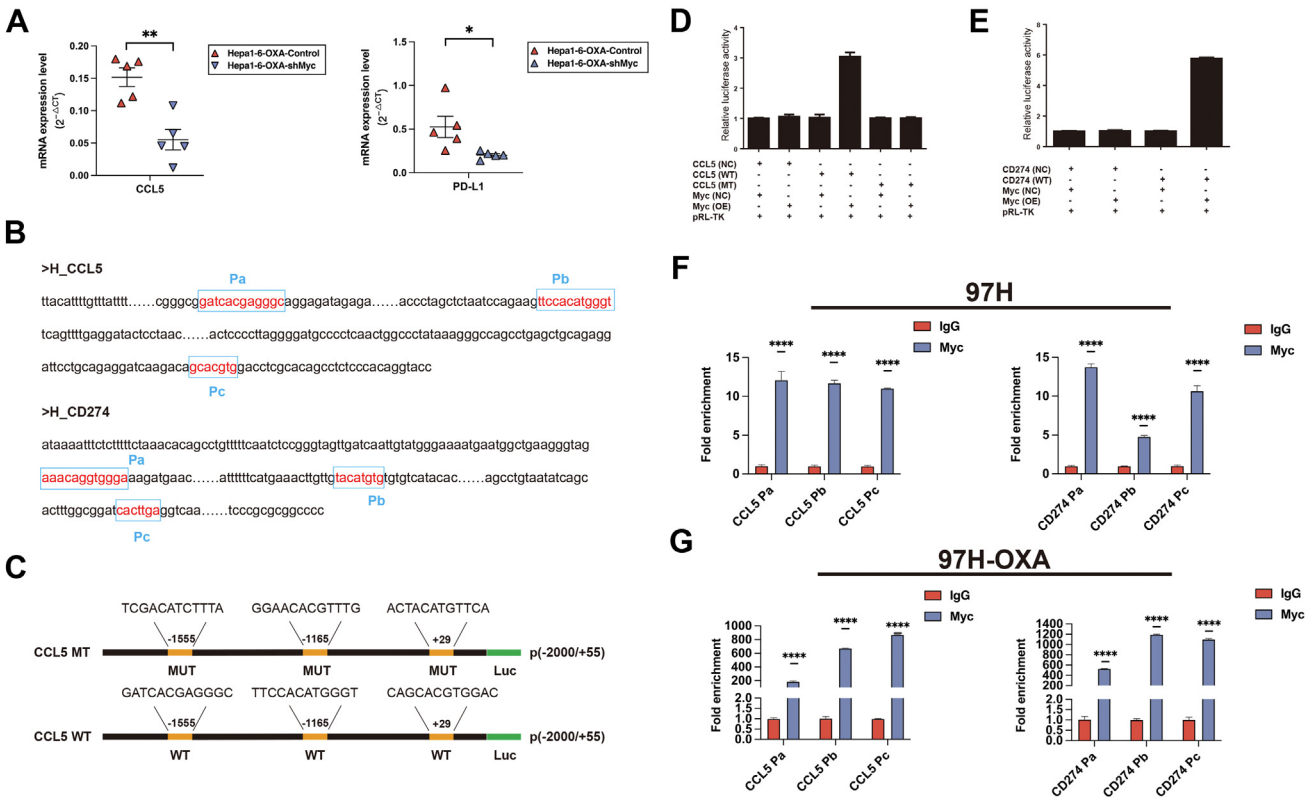

Figure 6. Myc induces CCL5 and PD-L1 overexpression via directly binding to their promoters. (*A*) The mRNA levels of CCL5 and PD-L1 in Hepa 1-6–control and Hepa 1-6–shMyc tumors were determined in vivo by qRT-PCR. (*B*) Illustration of potential Myc binding sites on CCL5 and PD-L1 (CD274) promoter regions, predicted using Jaspar and PROMO databases. (*C*) The WT CCL5/Luc promoter construct and mutant CCL5/Luc promoter construct with predicted potential binding sites mutated. (*D*) Dual luciferase reporter assay to analyze the activity of the WT or mutation pGL3-basic-CCL5 (−2000 to +55 bp) promoter constructs in human embryonic kidney-293 cells. Relative luciferase activities are shown (n = 3). (*E*) Dual luciferase reporter assay to analyze the activity of the pGL3-basic-CD274 (−1942 to +94 bp) promoter construct in human embryonic kidney-293 cells. Relative luciferase activities are shown (n = 3). (*F* and *G*) ChIP-qPCR assay verified the Myc binding sites on the promoter regions of CCL5 and PD-L1 in (*F*) 97H and (*G*) 97H-OXA cells. $^{*}P < .05$, $^{**}P < .01$, $^{***}P < .001$, and $^{****}P < .0001$. NC, negative control; OE, overexpression; pRL-TK, plasmid Renilla Luciferase–thymidine kinase.

oxaliplatin-resistant HCC. We also showed that ID1 conferred oxaliplatin resistance in HCC through regulating the proto-oncogene Myc.[19,28] Myc is well acknowledged as an essential gene product involved in the regulation of a multitude of cellular programs required for malignant growth. Recently, it was proposed that Myc regulates these programs in a manner that is coordinated with effects on the host tumor microenvironment and immune effectors.[17] However, it still is not clear how Myc influences the tumor microenvironment in oxaliplatin-resistant HCC. In this study, we report the significance and molecular mechanisms of the immunologic effects of ID-1/Myc signaling activation on the tumor microenvironment in oxaliplatin-resistant HCC.

MDSCs are a heterogeneous population of cells with potent immune regulatory activity, which can inhibit T-cell function and thus contribute to immune evasion in cancer.[11] A series of clinical and experimental studies have shown that the immunosuppression caused by the accumulation of MDSCs in the tumor microenvironment may be a key factor for the poor prognosis in HCC patients.[14,29–32] Furthermore, the value of MDSCs in predicting the therapeutic responses in cancer patients also has been proposed recently. The number of MDSCs is correlated negatively with the chemotherapy responses in uterine cervical cancer,[33] colorectal cancer,[34] and bladder cancer.[35] HCC patients with a high number of MDSCs after radiotherapy tend to have a decreased overall survival time.[36] It also has been suggested that the percentage of MDSCs is correlated negatively with the objective clinical response to ipilimumab (anti-CTLA4) and nivolumab (anti–PD-1) in melanoma.[37,38] Previous studies have explored in detail the essential role of MDSCs in HCC development and progression.[14,32] In the present study, we provide evidence that the accumulation of PMN-MDSCs in the spleens and tumor tissues in oxaliplatin-resistant HCC is associated with poor chemotherapy responses.

In the present study, we showed that the ID1/Myc signaling was activated in oxaliplatin-resistant HCC and correlated with PD-L1 up-regulation and PMN-MDSC infiltration in tumor tissues. The in vitro T-cell killing assays showed that oxaliplatin-resistant HCC cells were more resistant to activated $CD8^{+}$ T cells and this effect could be

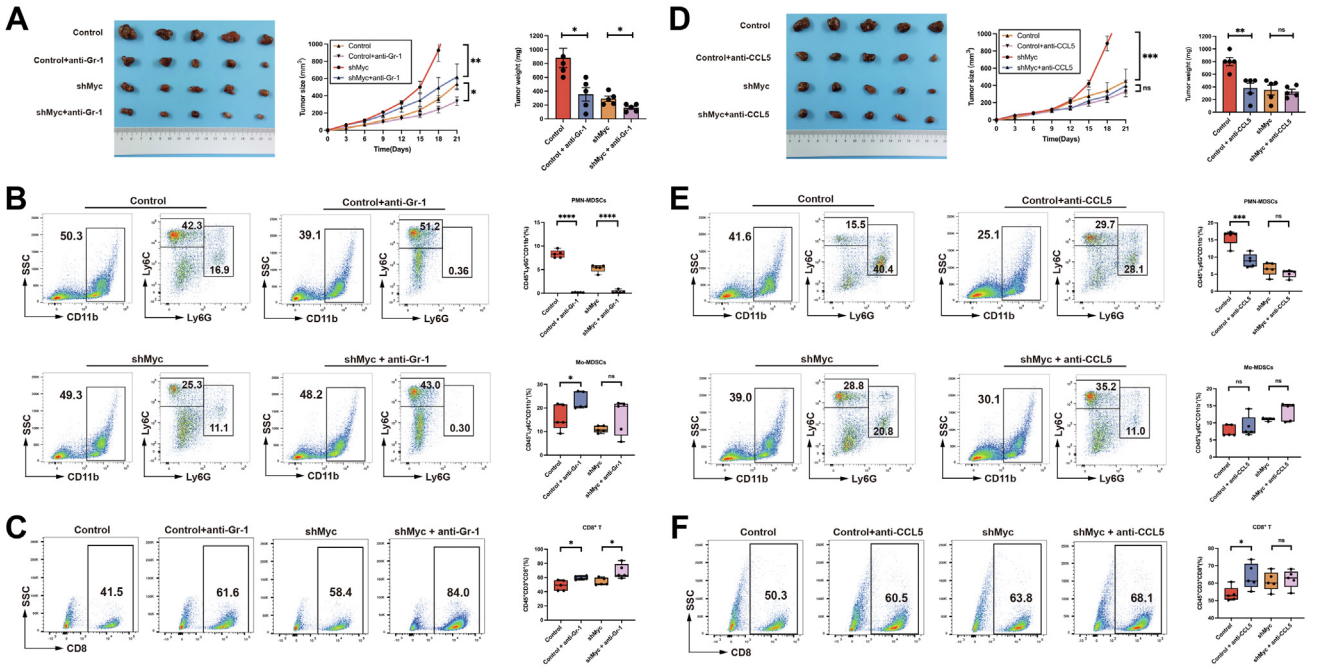

Figure 7. Blockage of CCL5 reverses PMN-MDSC chemotaxis promoted by ID1/Myc signaling to the oxaliplatin-resistant HCC. (*A*) Tumor growth curves and tumor weights of mice inoculated subcutaneously with Hepa 1-6–OXA–control cells or Hepa 1-6–OXA–shMyc cells, treated with anti–Gr-1 antibody (200 μg/mouse) or IgG every 48 hours from day 1 (n = 5 each). (*B* and *C*) Flow cytometric analysis of Hepa 1-6–OXA–control and Hepa 1-6–OXA–shMyc tumors treated with anti–Gr-1 antibody or IgG on day 21. The percentages of MDSCs and $CD8^+$ T cells are shown. (*D*) Tumor growth curves and tumor weights of mice inoculated subcutaneously with Hepa 1-6–OXA–control cells or Hepa 1-6–OXA–shMyc cells, treated with anti-CCL5 antibody (20 μg/mouse) or phosphate-buffered saline every 3 days from day 4 (n = 5 each). (*E* and *F*) Flow cytometric analysis of Hepa 1-6–OXA–control and Hepa 1-6–OXA–shMyc tumors treated with anti-CCL5 antibody or phosphate-buffered saline on day 21. The percentages of MDSCs and $CD8^+$ T cells are shown. *$P < .05$, **$P < .01$, ***$P < .001$, and ****$P < .0001$. SSC, side scatter.

abolished by Myc knockdown. In vivo studies also indicated that Myc deficiency decreased the frequencies of tumor-infiltrating PMN-MDSCs, but increased the frequencies of activated $CD8^+$ T cells in oxaliplatin-resistant HCC-bearing murine models. In the tumor sections, upon Myc knockdown, we also detected lower numbers of $CD11b^+$ myeloid cells, low levels of PD-L1 expression, and higher numbers of $CD8^+$ T cells, accompanied by HCC growth inhibition and increased apoptosis, as indicated by the Ki67 index and TUNEL assay. Together, these data showed that the activation of ID1/Myc signaling in oxaliplatin-resistant HCC induced PD-L1 up-regulation and PMN-MDSC accumulation, thus promoting tumor progression. The associations between Myc and PD-L1, and MDSC markers (CD11b and CD33) also were shown in 2 cohorts of HCC patients from public databases and 1 cohort from our center. In addition, Myc could serve as an excellent indicator of responses to adjuvant TACE in HCC patients.

To exclude the possibility that increased PMN-MDSCs were derived from myeloid cell conversion, we co-cultured bone marrow–derived cells with CM from Hepa 1-6 and Hepa 1-6–OXA cells, but no significant difference in MDSC induction was observed between the 2 groups. Next, we further confirmed that Myc overexpression facilitated PMN-MDSC recruitment by using a transwell migration assay in vitro. Because the Transwell system avoided direct contact between HCC cells and PMN-MDSCs, we speculated that the recruitment of PMN-MDSCs was mediated by the cytokines or chemokines secreted by oxaliplatin-resistant HCC cells. In previous studies, several chemokines were identified as important media for MDSC recruitment in the tumor microenvironment, among which chemokine (C-X-C motif) ligand (CXCL)1, CXCL2, and CXCL8 were identified as important chemokines in recruiting PMN-MDSCs, while CCL2 and CXCL12 were discovered to drive Mo-MDSC recruitment.[20] In this study, by using cytokine and chemokine qRT-PCR array, we characterized Myc-activated CCL5 up-regulation that drove PMN-MDSC recruitment in the tumor microenvironment. Actually, the dual luciferase reporter assay and ChIP-qPCR assay indicated that Myc could directly enhance CCL5 promoter activity and promote the transcription of CCL5. When the CCL5 was blocked by CCL5 antibody in vitro and in vivo, PMN-MDSC accumulation in the tumor microenvironment was dampened significantly. These results together indicated that Myc/CCL5 signaling was responsible for the recruitment of PMN-MDSCs.

MDSC depletion is a promising strategy to enhance antitumor immune responses and suppress tumor progression.[14,35,39] It has been shown that the Gr-1 neutralizing antibody could deplete primarily PMN-MDSCs in vivo.[35,40]

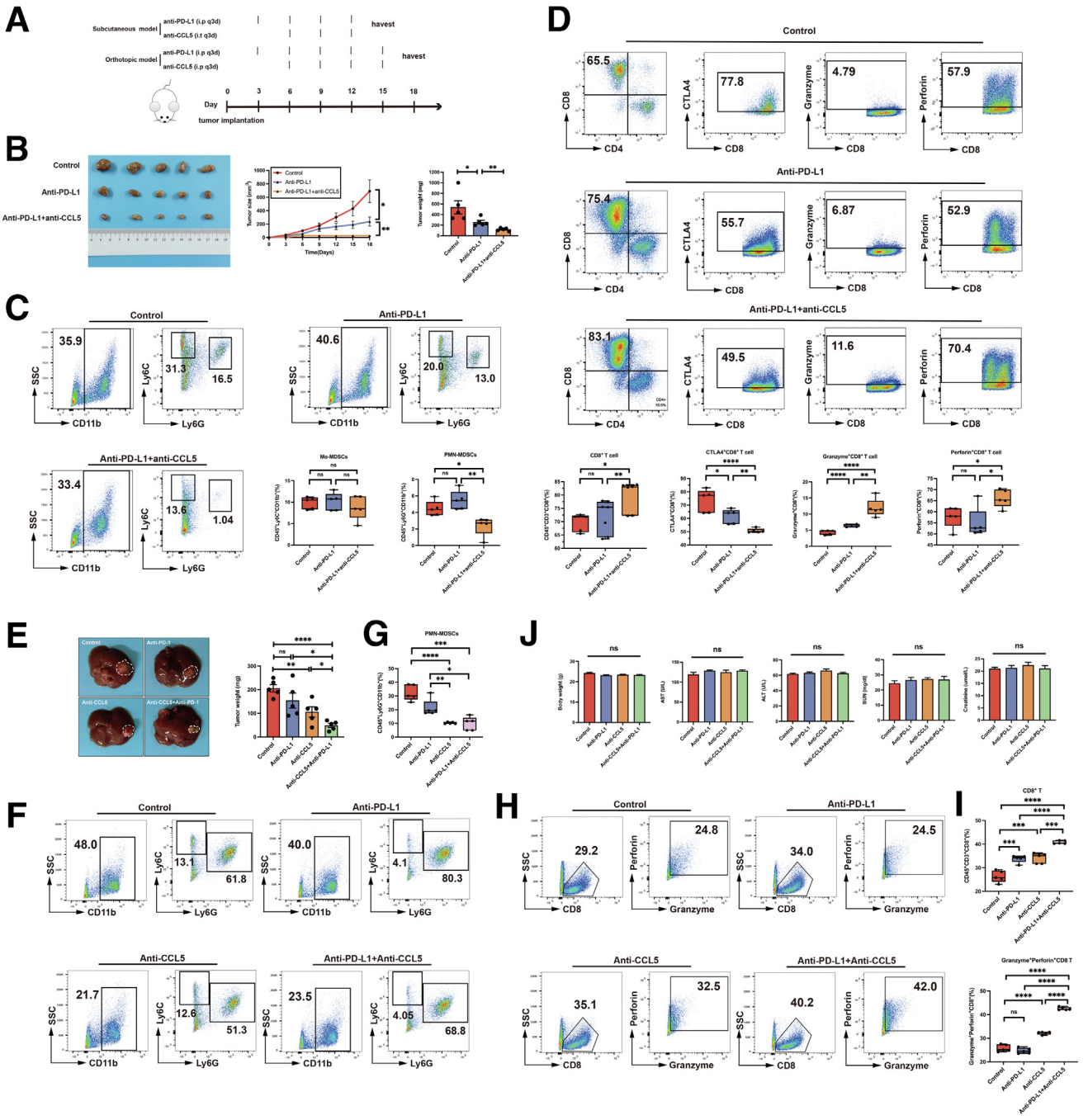

Figure 8. CCL-5 blockade enhances the antitumor effect of anti–PD-L1 treatment in oxaliplatin-resistant HCC. (*A*) The Hepa 1-6–OXA–bearing mice were randomized and treated with anti–PD-L1, anti-CCL5 combined with anti–PD-L1, or isotype control until the study end point. (*B*) Subcutaneous tumor growth curves and tumor weights of mice inoculated with Hepa 1-6–OXA cells, treated with anti–PD-L1, anti-CCL5 + anti–PD-L1, or isotype control (n = 5 each). (*C* and *D*) Flow cytometric analysis of Hepa 1-6–OXA tumors after anti–PD-L1 or combined with anti-CCL5 treatments on day 18. The percentages of MDSCs, $CD8^+$ T cells, and the expression levels of CTLA4, granzyme, and perforin in $CD8^+$ T cells are shown. (*E*) Orthotopic tumor weights of mice inoculated with Hepa 1-6–OXA cells, treated with anti–PD-L1, anti-CCL5, anti-CCL5 + anti–PD-L1, or isotype control (n = 5 each). (*F–I*) Flow cytometric analysis of Hepa 1-6–OXA tumors after anti–PD-L1, anti-CCL5, or combination treatments on day 15. The percentages of MDSCs, $CD8^+$ T cells, and the expression levels of granzyme and perforin in $CD8^+$ T cells are shown. (*J*) Quantitative analysis of body weight and indicated biochemistry indices for liver and kidney function after the experiments. $^*P < .05$, $^{**}P < .01$, $^{***}P < .001$, and $^{****}P < .0001$. ALT, alanine aminotransferase; AST, aspartate aminotransferase; BUN, blood urea nitrogen; SSC, side scatter.

However, unselective depletion of MDSCs may contribute to severe autoimmune disorders, and the absence of Ly6G in human beings also urges us to develop a clinical translation of this strategy. Because CCL5 has been identified as the core chemokine for PMN-MDSC accumulation in oxaliplatin-resistant HCC, it is reasonable to apply CCL5 neutralizing antibody to clinical practice to reverse immune evasion in oxaliplatin-resistant HCC. In addition, we found oxaliplatin-resistant HCC also presented with high expression of PD-L1. The combination of CCL5 neutralizing antibody and immune checkpoint inhibitors such as anti–PD-1/PD-L1 antibodies could be an effective strategy to tackle oxaliplatin-resistant HCC progression.

Conclusions

In conclusion, our study has shown that ID1/Myc activation in oxaliplatin-resistant HCC is responsible for chemoresistance as well as antitumor immune responses. Myc upregulation in oxaliplatin-resistant HCC promotes checkpoint molecular PD-L1 transcriptional expression and CCL5-induced PMN-MDSC chemotaxis, thus facilitating immune evasion and tumor progression. The use of CCL5 neutralizing antibody could reduce PMN-MDSC infiltration and suppress oxaliplatin-resistant HCC progression. To resolve the immune evasion in oxaliplatin-resistant HCC, the combined use of CCL5 neutralizing antibody and immune checkpoint inhibitors warrants further clinical trial validation.

Methods

Cell Lines

The human HCC cell line MHCC97H (high-metastasis) was established in the Liver Cancer Institute of Zhongshan Hospital.[41] The human HCC cell line Hep3B (low-metastasis) and murine HCC cell line Hepa 1-6 were purchased from the American Type Culture Collection. The oxaliplatin-resistant strains 97H-OXA, 3B-OXA, and Hepa 1-6–OXA cells were developed after 3 months of exposure to oxaliplatin (Sigma, St. Louis, MO), with stepwise increases to 15 μmol/L, 5 μmol/L, and 20 μmol/L, respectively. 97H, 97H-OXA, Hepa 1-6, and Hepa 1-6–OXA were cultured in Dulbecco's modified Eagle medium (Gibco/Invitrogen, Carlsbad, CA) supplemented with 10% fetal bovine serum (Gibco) and 1% penicillin-streptomycin (Invitrogen). 3B and 3B-OXA were cultured in minimum essential medium supplemented with 10% fetal bovine serum and 1% penicillin-streptomycin.

Cell Viability Assay

Oxaliplatin cytotoxicity and resistance were evaluated using the CCK-8 assay (Yeasen, Shanghai, China). Briefly, cells were seeded into 96-well plates (5000 cells/well). After incubation for 24 hours, oxaliplatin was administered at various concentrations for 72 hours. Then, 10 μL CCK-8 reagent was added to each well and incubated at 37°C for 2 hours. The absorbance was measured using a Multiskan Spectrum spectrophotometer (Thermo Scientific) at a wavelength of 450 nm.

RNA extraction and Real-Time qPCR

Total RNA was extracted from cells by the RNA-Quick Purification Kit (EZBioscience, China) and reverse transcribed into complementary DNA using the 4× EZscript Reverse Transcription Mix II (EZBioscience). For qPCR analysis, single-stranded complementary DNA was amplified using a 2× SYBR Green qPCR Master Mix (ROX2 plus; EZBioscience). β-actin was used as an internal control. All reactions were performed in triplicate. Primer sequences are listed in Table 2.

Immunoblotting

Samples were treated with radioimmunoprecipitation assay lysis buffer supplemented with phenylmethanesulfonyl fluoride (Beyotime, China). Then, cell lysates were centrifuged (14,000 rpm for 20 minutes at 4°C), quantified by BCA protein assay (Beyotime), and boiled for 5–10 minutes. A total of 20 ug protein was resolved by 10% sodium dodecyl sulfate–polyacrylamide gel electrophoresis and electroblotted onto polyvinylidene difluoride membranes (0.2 μm; Millipore). After blocking with QuickBlock Blocking Buffer for Western Blot (Beyotime) for 15 minutes, membranes were incubated with primary antibodies at 4°C overnight, followed by secondary antibodies for 2 hours at room temperature. Primary antibodies used were glyceraldehyde-3-phosphate dehydrogenase Mouse Monoclonal Antibody (Beyotime), anti-ID1 antibody (ab230679), anti-Myc antibody (ab32072), and anti–PD-L1 antibody (ab205921 for human beings; ab213480 for mice). Protein bands were visualized by using Ncm-ECL Ultra (New Cell and Molecular Biotech Co, Ltd, China).

Transfection of Lentiviral Vectors With Small Hairpin RNAs for Myc

97H-OXA-shMyc-1/2 and Hep3B-OXA-shMyc-1/2 with stable Myc knockdown were generated using human lentiviral small hairpin RNA (shRNA) viral particles (Genomeditech, Shanghai, China; gene target sequence was as follows: shMyc-1, GGAAGAAATCGATGTTGTTTC; shMyc-2, GGAAACGACGAGAACAGTTGA). Hepa 1-6–OXA–shMyc-1/2 cells were generated using mouse lentiviral shRNA viral particles (Genomeditech; gene target sequence was as follows: shMyc-1, GCGACGAGGAAGAGAATTTCT; shMyc-2, GGAGATGATGACCGAGTTACT). Control cell lines 97H-OXA-control, Hep3B-OXA-control, and Hepa 1-6–OXA–control were generated through the transfection of nonsilencing, control shRNAs (Genomeditech). After transfection for 48 hours, cells were selected in culture medium with 6 μg/mL puromycin for 48 hours. The efficiency of gene silencing was confirmed by qRT-PCR and Western blot analysis.

ELISA

Human CCL5 protein levels in culture supernatants were measured using the Human CCL5/regulated upon

Table 1. Clinical Characteristics of HCC Patients in the Zhongshan Cohort Before and After Propensity Score Matching

Characteristics	Before matching			After matching		
	Without TACE (n = 298)	Postoperative TACE (n = 54)	*P* value	Without TACE (n = 49)	Postoperative TACE (n = 49)	*P* value
Age, *y*	51.9 ± 11.2	51.9 ± 10.7	.995	51.5 ± 10.6	52.1 ± 10.6	.790
Sex, female/male	49/249	8/46	.765	6/43	7/42	.766
History of hepatitis	12.4 ± 15.3	14.8 ± 19.3	.319	16.2 ± 23.0	13.4 ± 15.8	.479
Liver cirrhosis, absence/presence	285/13	54/0	.118	49/0	49/0	1.000
Family history of liver cancer, absence/presence	287/11	52/2	.063	48/1	47/2	.503
HBsAg, positive/negative	43/255	3/51	.183	2/47	3/46	.646
HBcAb, positive/negative	13/285	0/54	.294	0/49	0/49	1.000
HCV antibody, positive/negative	9/289	1/53	.634	1/48	1/48	1.000
TB, *umol/L*	12.5 ± 5.3	13.4 ± 5.8	.235	13.5 ± 6.3	13.3 ± 5.8	.896
ALT, *U/L*	39.0 ± 22.0	37.6 ± 18.1	.639	38.0 ± 21.3	38.5 ± 18.7	.900
ALB, *g/L*	4.0 ± 0.4	4.0 ± 0.4	.663	4.0 ± 0.3	4.0 ± 0 .4	.804
AFP, *ng/mL*	4989.5 ± 13,781.7	8906.9 ± 18,265.7	.070	9385.8 ± 18,938.8	8058.3 ± 17,555.5	.720
PTT, *s*	12.4 ± 1.1	12.5 ± 1.3	.310	12.7 ± 1.1	12.5 ± 1.2	.324
γ-GT, *U/L*	83.0 ± 87.6	107.6 ± 88.4	.059	105.8 ± 122.7	107.7 ± 91.7	.930
Tumor size, *cm*	5.3 ± 3.0	7.1 ± 3.1	<.001[a]	6.9 ± 3.3	6.8 ± 3.0	.919
Tumor number, single/multiple	275/23	47/7	.285	42/7	42/7	1.000
Cirrhotic nodules, 0/1/2/3	9/51/124/114	1/12/22/19	.799	1/6/22/20	1/12/18/18	.474
Tumor capsule, complete / incomplete	149/149	20/34	.079	14/35	19/30	.285
Tumor differentiation, I/II/III/IV	2/232/63/1	0/32/22/0	.019[a]	0/35/13/1	0/31/18/0	.359
TNM stage, I/II/III	187/110/1	28/26/0	.277	26/22/1	27/22/0	.601
Vascular invasion, absence/ presence	210/88	20/34	<.001[a]	24/25	18/31	.221

AFP, alfa-fetoprotein; ALB, albumin; ALT, alanine aminotransferase; γ-GT, γ-glutamyl transpeptidase; HBcAb, antibody to hepatitis B core antigen; HBsAg, hepatitis B virus surface antigen; HCV, hepatitis C virus; PPT, partial thromboplastin time; TB, total bilirubin.
[a]Statistically significant.

activation,normal T-cell espressed and secreted (RANTES) Quantikine ELISA Kit (R&D Systems, Minneapolis, MN) according to the manufacturer's protocols. Mouse CCL5 protein levels were measured using the Mouse/Rat CCL5/RANTES Quantikine ELISA Kit (R&D Systems) according to the manufacturer's protocols.

Immunohistochemistry

Formalin-fixed, paraffin-embedded sections (5 μm) were deparaffinized with xylene, rehydrated with a graduated series of ethanol, and rinsed with distilled water. Antigen retrieval was performed in EDTA buffer by boiling. The endogenous peroxidase activity was blocked with 3% hydrogen peroxide in methanol for 30 minutes. After normal goat serum block, sections were stained with primary antibodies against CD8α (ab209775; Abcam), CD11b (ab133357; Abcam), PD-L1 (human: GB11339; Servicebio; mouse: 13684; Cell Signaling Technology), Myc (GB13076; Servicebio), ID1 (GB11182; Servicebio), and Ki67 (GB111141; Servicebio), overnight at 4°C, followed by incubation with the horseradish-peroxidase–conjugated secondary antibodies (Dako) for 30 minutes at room temperature. Sections were visualized with 3, 3′-diaminobenzidine (Sigma-Aldrich) and counterstained with hematoxylin. The cell apoptosis was detected using a 3,3′-diaminobenzidine tetra hydrochloride Streptavidin-Horseradish Peroxidase (SA-HRP) TUNEL Cell Apoptosis Detection Kit (G1507; Servicebio).

qRT-PCR Array

The cytokines and chemokines PCR array was performed to screen hepatoma-derived cytokines/chemokines according to the manufacturer's protocol (Wcgene Biotech, Shanghai, China). The gene expression data were analyzed using Wcgene Biotech software. The relative gene expression levels of target genes were calculated using the $2^{-\Delta\Delta Ct}$ method.[42,43]

Dual Luciferase Reporter Assay

Human embryonic kidney-293 cells were cultured in 24-well plates and co-transfected with firefly luciferase reporter gene constructs, hRluc-CMV vector, and pcDNA3.1 control or pcDNA3.1-Myc expression plasmid when cells

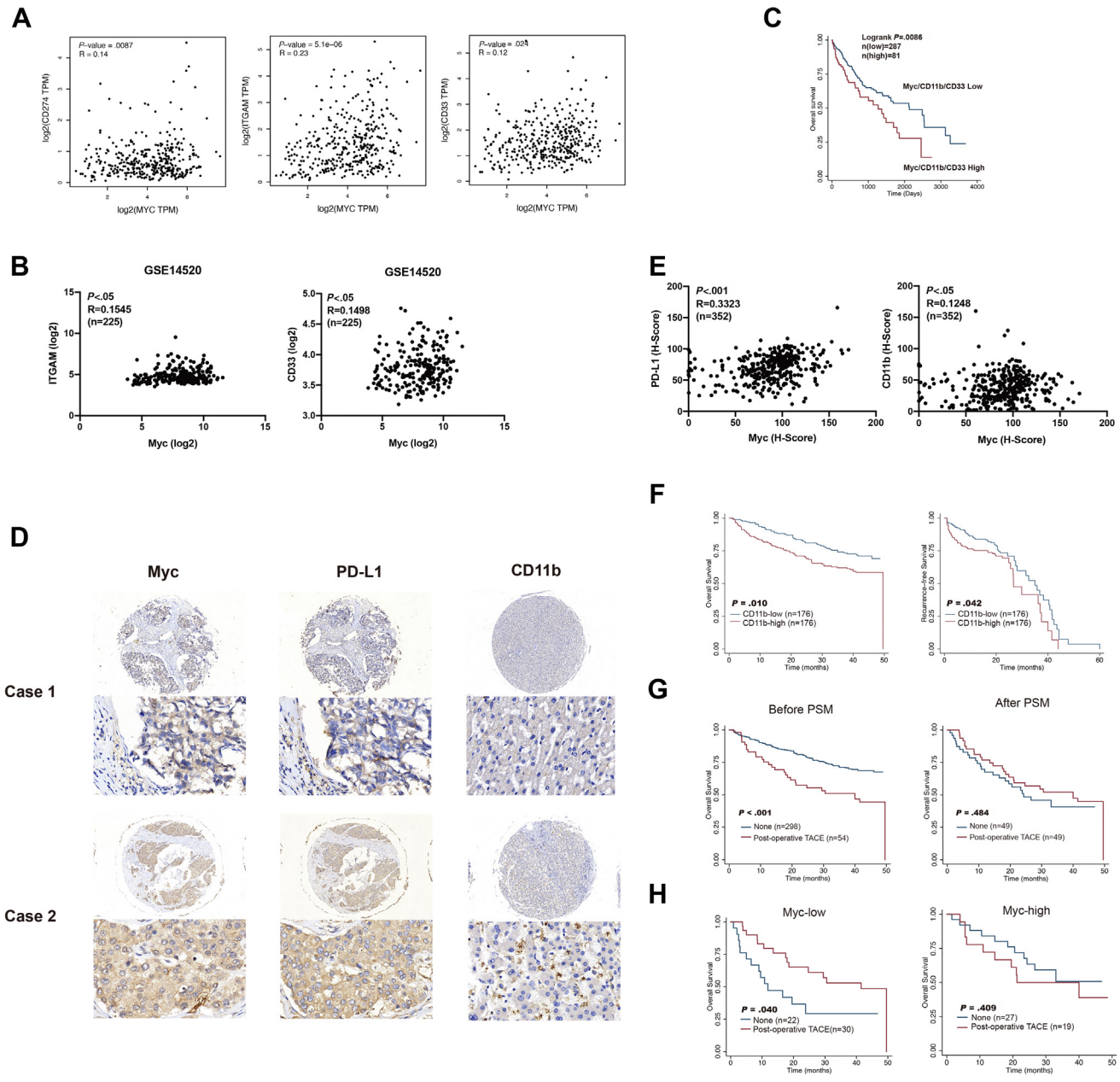

Figure 9. The prognostic values and correlations of Myc, PD-L1, and MDSC markers in HCC. (*A*) Correlation analysis between Myc and PD-L1, MDSC markers (CD11b, CD33) using gene expression data from the TCGA data set. (*B*) Correlation analysis between Myc and MDSC markers (CD11b, CD33) using gene expression data from the GEO data set (GSE14520). (*C*) Kaplan–Meier overall survival curves of HCC patients with high or low expressions (stratified by median) of Myc/CD11b/CD33. (*D*) Representative pictures of immunohistochemical staining of Myc, PD-L1, and CD11b in the patient HCC tissues are shown (N = 352; magnification, ×100). (*E*) The associations between H-scores of PD-L1, CD11b, and Myc are shown in the 352 patients with HCC. (*F*) Kaplan–Meier overall survival and recurrence-free survival curves of HCC patients with high or low expressions (stratified by median) of CD11b. (*G*) Kaplan–Meier overall survival curves of HCC patients receiving or not receiving postoperative adjuvant TACE before and after PSM. (*H*) Kaplan–Meier overall survival curves of HCC patients receiving or not receiving postoperative adjuvant TACE in the low and high Myc groups after PSM. *$P < .05$, **$P < .01$, ***$P < .001$, and ****$P < .0001$. ITGAM, integrin subunit alpha M; TPM, transcripts per kilobase million.

reached 70% confluence. The CCL5 (NM_002985) and CD274 (NM_014143) promoter regions were cloned by gene synthesis in accordance with coding sequences, and were inserted into pGL3-basic vectors (WT). The pGL3-basic-CCL5 promoter (MT) was constructed based on the potential binding sites between Myc and CCL5 promoter predicted using Jaspar and PROMO databases.[44,45] After 48 hours, the firefly (pGL3) and Renilla luciferase activities were measured with the Dual Luciferase Reporter Assay System (Promega) according to the manufacturer's instructions. The relative

Table 2. Primers Used for Quantitative Real-Time PCR in This Study

Name	Forward sequence, 5' to 3'	Reverse sequence, 3' to 5'
Human β-actin	CATGTACGTTGCTATCCAGGC	CTCCTTAATGTCACGCACGAT
Human ID1	CTGCTCTACGACATGAACGG	GAAGGTCCCTGATGTAGTCGAT
Human c-Myc	GGCTCCTGGCAAAAGGTCA	CTGCGTAGTTGTGCTGATGT
Human PD-L1	TGGCATTTGCTGAACGCATTT	TGCAGCCAGGTCTAATTGTTTT
Human CCL5	CAGTCGTCTTTGTCACCCGA	CGGGTGGGGTAGGATAGTGA
Mouse β-actin	GGCTGTATTCCCCTCCATCG	CCAGTTGGTAACAATGCCATGT
Mouse ID1	CCTAGCTGTTCGCTGAAGGC	GTAGAGCAGGACGTTCACCT
Mouse c-Myc	CCCTATTTCATCTGCGACGAG	GAGAAGGACGTAGCGACCG
Mouse PD-L1	GCTCCAAAGGACTTGTACGTG	TGATCTGAAGGGCAGCATTTC
Mouse CCL5	GCTGCTTTGCCTACCTCTCC	TCGAGTGACAAACACGACTGC

activity of different promoters was defined as the ratio of firefly luciferase/Renilla luciferase.

ChIP Assay

For chromatin immunoprecipitation, 1×10^7 97H and 97H-OXA cells were fixed with 1% formaldehyde, lysed, and sonicated to shear chromatin DNA. Sheared DNA fragments were immunoprecipitated with anti-Myc antibody (ab32072; Abcam) and IgG control. The enrichment of target sequences in ChIP material was determined by PCR reactions in triplicate. Forward and reverse primer sequences used for ChIP-qPCR are listed in Table 3.

Preparation of Single-Cell Suspensions

Before flow cytometry analysis and magnetic bead cell sorting, single-cell suspensions were prepared. Tumors collected from Hepa 1-6–bearing C57BL/6 mice were dissected and finely minced on a programmable gentleMACS dissociator (Miltenyi Biotech) and digested with an enzyme solution containing collagenase IV (0.2 mg/mL) and DNase I (10 μg/mL; Sigma-Aldrich). The single-cell suspension was obtained by passing through a 70-μm cell mesh and resuspended in Hank's buffer. Mouse spleens were pressed through a 40-μm cell mesh using a syringe plunger to obtain a single-cell suspension. The red blood cells in cell preparations and whole blood were removed using ACK Lysing Buffer (Gibco).

Flow Cytometric Analysis

Cells were incubated with Fc receptors block for 10 minutes at room temperature and stained with fluorescence-conjugated monoclonal antibodies specific to mouse immune cell surface markers for 30 minutes at 4°C. After surface staining, the cells were resuspended in Fixation/Permeabilization solution (BD Biosciences) and incubated for 20 minutes at 4°C. Intracellular staining (anti-mouse FoxP3 and IFN-γ antibodies) was performed according to the manufacturer's protocol. The antibodies used are listed in Table 4. Labeled cells were washed with fluorescence activated cell sorting (FACS) buffer twice and analyzed using a BD FACSCantoII Analyzer (BD Biosciences) and FlowJo software (version 10.4).

MDSC Isolation by Magnetic Bead Cell Sorting

Isolation of $CD11b^+Ly6G^+$ PMN-MDSCs was performed using a mouse MDSC isolation kit (Miltenyi Biotec, FL) according to the manufacturer's instructions. Briefly, after FcR blocking, cells were stained by anti–Ly6G–biotin antibody and labeled with antibiotin microbeads. The cell suspension was passed through an LS separation column (Miltenyi Biotec) and the retained cells were the purified murine MDSCs ($CD11b^+Gr\text{-}1^{hi}Ly6G^+$ population).

PMN-MDSC Transwell Migration Assay

In vitro migration of murine PMN-MDSCs was evaluated in 24-well plates with Transwell polycarbonate-permeable supports (8.0 μm; Costar Corning, Cambridge, MA). Freshly isolated splenic PMN-MDSCs (1×10^6) were seeded in the upper chambers of the inserts. The CM from Hepa 1-6, Hepa 1-6–OXA, Hepa 1-6–OXA–control, and Hepa 1-6–OXA–shMyc were placed in the lower chamber. The mouse CCL5 antibody was placed in the lower chamber at a concentration of 10 μg/mL (R&D Systems). After incubation for 36 hours, the number of PMN-MDSCs in the bottom compartment was counted.

T-Cell Proliferation Assay

$CD8^+$ T cells were obtained from splenocytes of WT C57BL/6 mice using a mouse T-cell isolation kit (Stem Cell Technologies), and were stained with carboxyfluorescein succinimidyl ester (2.5 μmol/L; Invitrogen, MA). Isolated MDSCs were co-cultured with T cells in 96-well plates with mouse T-activator CD3/CD28 beads (beads:T cells = 1:10; Gibco) and mouse interleukin 2 (10 ng/mL; BioLegend) at various ratios. After 72 hours, the T-cell proliferation rates were evaluated by flow cytometry.

T-Cell–Mediated Tumor-Killing Assay

Human peripheral blood mononuclear cells were cultured in ImmunoCult-XF T-cell Expansion Medium (10981; Stemcell Technologies) with ImmunoCult Human CD3/CD28/CD2

Table 3. Primers used for Chromatin Immunoprecipitation (ChIP) Analyses

Name	Forward sequence, 5' to 3'	Reverse sequence, 3' to 5'
Human CCL5-1	TTAAATAATTCAGATGCCGGCC	CCATGTTAGCCAGGATGGTC
Human CCL5-2	GAAGACTTACTGTATCCAGTTC	GTGCTCTGTCCATTAAGTAC
Human CCL5-3	TGAGCTGCAGAGGATTCCTG	GCAGTAGCAATGAGGATGACAG
Human CD274-1	CGGGTAGTTGATCAATTGTATG	CTTGCTGCTCAGTGATTTG
Human CD274-2	GGGCATTGCAGATAGTAGATC	CCAACTTTGGTGACTGTGAC
Human CD274-3	GAAAAGGGAGCACACAGGCA	GCTGAACTTCTAGGTGCTCTC

T-cell Activator (10970; Stemcell Technologies) and recombinant human interleukin 2 protein (1000 U/mL, 202-IL-050; R&D Systems) for 1 week according to the manufacturer's protocol to acquire activated T cells. HCC cells were allowed to adhere to the plates overnight and then co-cultured with activated T cells at a 1:3 ratio for 48 hours. Finally, T cells and cell debris were removed by a phosphate-buffered saline wash, and living cancer cells were quantified by a CCK-8 assay.

Animal Experiments

For this study, 6- to 8-week-old male C57BL/6 mice were purchased from SLAC Laboratory Animal Co, Ltd (Shanghai, China). For subcutaneous tumor models, a total of 5×10^6 HCC cells were inoculated into the right flank of the mice. The mice were monitored every 3 days and the tumor volumes were measured using the following formula: length $\times$ width^2 $\times$ 0.5 (mm^3). For orthotopic tumor xenograft models, tumors from subcutaneous tumor tissues were minced into 2-mm^3 cubes and transplanted to the livers of WT C57BL/6 mice. At the study end point, the weight of each tumor was assessed. For drug treatment, the tumor-bearing mice were treated with 10 mg/kg oxaliplatin (Sigma, St. Louis, MO) intraperitoneally (IP) weekly for up to 21 days. To evaluate the efficacy of PD-L1 and MDSC blockade on oxaliplatin-resistant HCC, Hepa 1-6–OXA–control or Hepa 1-6–OXA–shMyc–bearing mice were treated with anti–Gr-1 antibody (200 μg/mouse, IP, every 3 days; Bio X cell, NH), anti-CCL5 antibody (20 ug/mouse, intratumorally, every 3 days; R&D Systems), or anti–PD-L1 antibody (200 μg, IP, every 3 days; Bio X cell). The control mice were treated with an isotype control antibody (Bio X cell) or vehicle (phosphate-buffered saline). The mice were killed humanely after treatments and the blood, spleen, and tumor samples were collected for analysis.

Table 4. Antibodies Used for Flow Cytometry

Antibody	Clone	Company
Anti-CD45	30-F11	BioLegend
Anti-CD11b	M1/70	BD
Anti–Gr-1	RB6-8C5	BioLegend
Anti-CD8	53-6.7	eBioscience
Anti-Ly6C	HK1.4	BioLegend
Anti-Ly6G	1A8	BioLegend
Anti-CD3	145-2C11	eBioscience
Anti-CD4	RM4-5	eBioscience
Anti-CD25	PC61.5	eBioscience
Anti-FoxP3	FJK-16s	eBioscience
Anti-F4/80	BM8	BioLegend
Anti–IFN-γ	XMG1.2	BioLegend
Anti-CD274	MIH1	Invitrogen
Anti–granzyme B	QA16A02	BioLegend
Anti-CTLA4	UC10-4B9	BioLegend
Anti–Tim-3	B8.2C12	BioLegend
Antiperforin	S16009A	BioLegend

Clinical Tissue Samples

HCC tissue microarrays were used in this study. A total of 352 formalin-fixed, paraffin-embedded HCC tissues (containing tumor and adjacent normal tissues) were included. These tissues were collected from consecutive HCC patients who underwent curative resection at the Liver Cancer Institute, Fudan University (Shanghai, China) (Table 1). Written informed consent was obtained, and samples were used with approval from the Institutional Review Board of Zhongshan Hospital, Fudan University (B2022-164).

Ethics Statements

The study protocol was approved by the Medical Ethics Committee of Zhongshan Hospital, affiliated with Fudan University. The study was performed in accordance with the Helsinki Declaration. All animal studies were approved by the Ethical Committee on Animal Experiments of the Animal Care Committee of Zhongshan Hospital of Fudan University and performed according to the Shanghai Medical Experimental Animal Care Commission Guidelines.

Statistical Analysis

Results are shown as the means $\pm$ SEM. Comparisons between 2 groups were performed using Student t tests. The multivariate analysis was performed using the Cox proportional hazards regression model and the log-rank test was used for survival analysis. All statistical analyses were performed using STATA (version 15.1; StataCorp, College Station, TX) and GraphPad Prism 6.

References

1. Forner A, Reig M, Bruix J. Hepatocellular carcinoma. Lancet 2018;391:1301–1314.

2. Zhu RX, Seto WK, Lai CL, Yuen MF. Epidemiology of hepatocellular carcinoma in the Asia-Pacific region. Gut Liver 2016;10:332–339.
3. European Association for the Study of the Liver. EASL clinical practice guidelines: management of hepatocellular carcinoma. J Hepatol 2018;69:182–236.
4. Qin S, Bai Y, Lim HY, et al. Randomized, multicenter, open-label study of oxaliplatin plus fluorouracil/leucovorin versus doxorubicin as palliative chemotherapy in patients with advanced hepatocellular carcinoma from Asia. J Clin Oncol 2013;31:3501–3508.
5. Kelland L. The resurgence of platinum-based cancer chemotherapy. Nat Rev Cancer 2007;7:573–584.
6. Zhu H, Shan Y, Ge K, et al. Oxaliplatin induces immunogenic cell death in hepatocellular carcinoma cells and synergizes with immune checkpoint blockade therapy. Cell Oncol (Dordr) 2020;43:1203–1214.
7. Wen L, Liang C, Chen E, et al. Regulation of multi-drug resistance in hepatocellular carcinoma cells is TRPC6/calcium dependent. Sci Rep 2016;6:23269.
8. Martinez-Balibrea E, Martínez-Cardús A, Ginés A, et al. Tumor-related molecular mechanisms of oxaliplatin resistance. Mol Cancer Ther 2015;14:1767–1776.
9. Liu Z, Lin Y, Zhang J, et al. Molecular targeted and immune checkpoint therapy for advanced hepatocellular carcinoma. J Exp Clin Cancer Res 2019;38:447.
10. Rogovskii VS. The linkage between inflammation and immune tolerance: interfering with inflammation in cancer. Curr Cancer Drug Targets 2017;17:325–332.
11. Veglia F, Perego M, Gabrilovich D. Myeloid-derived suppressor cells coming of age. Nat Immunol 2018;19:108–119.
12. Bronte V, Brandau S, Chen SH, et al. Recommendations for myeloid-derived suppressor cell nomenclature and characterization standards. Nat Commun 2016;7:12150.
13. Kumar V, Patel S, Tcyganov E, Gabrilovich DI. The nature of myeloid-derived suppressor cells in the tumor microenvironment. Trends Immunol 2016;37:208–220.
14. Li YM, Liu ZY, Wang JC, et al. Receptor-interacting protein kinase 3 deficiency recruits myeloid-derived suppressor cells to hepatocellular carcinoma through the chemokine (C-X-C Motif) ligand 1-chemokine (C-X-C Motif) receptor 2 axis. Hepatology 2019;70:1564–1581.
15. Zhao Z, Bo Z, Gong W, Guo Y. Inhibitor of differentiation 1 (Id1) in cancer and cancer therapy. Int J Med Sci 2020;17:995–1005.
16. Shachaf CM, Kopelman AM, Arvanitis C, et al. MYC inactivation uncovers pluripotent differentiation and tumour dormancy in hepatocellular cancer. Nature 2004;431:1112–1117.
17. Casey SC, Baylot V, Felsher DW. The MYC oncogene is a global regulator of the immune response. Blood 2018;131:2007–2015.
18. Casey SC, Tong L, Li Y, et al. MYC regulates the antitumor immune response through CD47 and PD-L1. Science 2016;352:227–231.
19. Yin X, Tang B, Li JH, et al. ID1 promotes hepatocellular carcinoma proliferation and confers chemoresistance to oxaliplatin by activating pentose phosphate pathway. J Exp Clin Cancer Res 2017;36:166.
20. Li BH, Garstka MA, Li ZF. Chemokines and their receptors promoting the recruitment of myeloid-derived suppressor cells into the tumor. Mol Immunol 2020;117:201–215.
21. Chong CC, Cheung ST, Cheung YS, et al. Novel biomarkers GEP/ABCB5 regulate response to adjuvant transarterial chemoembolization after curative hepatectomy for hepatocellular carcinoma. Hepatobiliary Pancreat Dis Int 2018;17:524–530.
22. Zhang Y, Tang B, Song J, et al. Lnc-PDZD7 contributes to stemness properties and chemosensitivity in hepatocellular carcinoma through EZH2-mediated ATOH8 transcriptional repression. J Exp Clin Cancer Res 2019;38:92.
23. Cao H, Phan H, Yang LX. Improved chemotherapy for hepatocellular carcinoma. Anticancer Res 2012;32:1379–1386.
24. Matsuda Y, Yamagiwa S, Takamura M, et al. Overexpressed Id-1 is associated with a high risk of hepatocellular carcinoma development in patients with cirrhosis without transcriptional repression of p16. Cancer 2005;104:1037–1044.
25. Ao J, Meng J, Zhu L, et al. Activation of androgen receptor induces ID1 and promotes hepatocellular carcinoma cell migration and invasion. Mol Oncol 2012;6:507–515.
26. Li L, Wei X, Wu B, et al. siRNA-mediated knockdown of ID1 disrupts Nanog- and Oct-4-mediated cancer stem cell-likeness and resistance to chemotherapy in gastric cancer cells. Oncol Lett 2017;13:3014–3024.
27. Przybyla T, Sakowicz-Burkiewicz M, Maciejewska I, et al. Suppression of ID1 expression in colon cancer cells increases sensitivity to 5-fluorouracil. Acta Biochim Pol 2017;64:315–322.
28. Bu Y, Jia QA, Ren ZG, et al. Maintenance of stemness in oxaliplatin-resistant hepatocellular carcinoma is associated with increased autocrine of IGF1. PLoS One 2014;9:e89686.
29. Elwan N, Salem ML, Kobtan A, et al. High numbers of myeloid derived suppressor cells in peripheral blood and ascitic fluid of cirrhotic and HCC patients. Immunol Invest 2018;47:169–180.
30. Hetta HF, Zahran AM, Mansor SG, et al. Frequency and implications of myeloid-derived suppressor cells and lymphocyte subsets in Egyptian patients with hepatitis C virus-related hepatocellular carcinoma. J Med Virol 2019;91:1319–1328.
31. Lee WC, Wang YC, Cheng CH, et al. Myeloid-derived suppressor cells in the patients with liver resection for hepatitis B virus-related hepatocellular carcinoma. Sci Rep 2019;9:2269.
32. Zhou J, Liu M, Sun H, et al. Hepatoma-intrinsic CCRK inhibition diminishes myeloid-derived suppressor cell immunosuppression and enhances immune-checkpoint blockade efficacy. Gut 2018;67:931–944.
33. Kawano M, Mabuchi S, Matsumoto Y, et al. The significance of G-CSF expression and myeloid-derived suppressor cells in the chemoresistance of uterine cervical cancer. Sci Rep 2015;5:18217.

34. Tada K, Kitano S, Shoji H, et al. Pretreatment immune status correlates with progression-free survival in chemotherapy-treated metastatic colorectal cancer patients. Cancer Immunol Res 2016;4:592–599.
35. Takeyama Y, Kato M, Tamada S, et al. Myeloid-derived suppressor cells are essential partners for immune checkpoint inhibitors in the treatment of cisplatin-resistant bladder cancer. Cancer Lett 2020;479:89–99.
36. Wang D, An G, Xie S, et al. The clinical and prognostic significance of CD14(+)HLA-DR(-/low) myeloid-derived suppressor cells in hepatocellular carcinoma patients receiving radiotherapy. Tumour Biol 2016; 37:10427–10433.
37. de Coaña YP, Wolodarski M, Poschke I, et al. Ipilimumab treatment decreases monocytic MDSCs and increases CD8 effector memory T cells in long-term survivors with advanced melanoma. Oncotarget 2017;8:21539–21553.
38. Weber J, Gibney G, Kudchadkar R, et al. Phase I/II study of metastatic melanoma patients treated with nivolumab who had progressed after ipilimumab. Cancer Immunol Res 2016;4:345–353.
39. Taki M, Abiko K, Baba T, et al. Snail promotes ovarian cancer progression by recruiting myeloid-derived suppressor cells via CXCR2 ligand upregulation. Nat Commun 2018;9:1685.
40. Qin H, Lerman B, Sakamaki I, et al. Generation of a new therapeutic peptide that depletes myeloid-derived suppressor cells in tumor-bearing mice. Nat Med 2014;20:676–681.
41. Li Y, Tian B, Yang J, et al. Stepwise metastatic human hepatocellular carcinoma cell model system with multiple metastatic potentials established through consecutive in vivo selection and studies on metastatic characteristics. J Cancer Res Clin Oncol 2004;130:460–468.
42. Tarca AL, Romero R, Draghici S. Analysis of microarray experiments of gene expression profiling. Am J Obstet Gynecol 2006;195:373–388.
43. Livak KJ, Schmittgen TD. Analysis of relative gene expression data using real-time quantitative PCR and the 2(-delta delta C(T)) method. Methods 2001;25:402–408.
44. Fornes O, Castro-Mondragon JA, Khan A, et al. JASPAR 2020: update of the open-access database of transcription factor binding profiles. Nucleic Acids Res 2020; 48:D87–D92.
45. Netanely D, Stern N, Laufer I, Shamir R. PROMO: an interactive tool for analyzing clinically-labeled multi-omic cancer datasets. BMC Bioinformatics 2019;20:732.

Received April 7, 2022. Accepted December 6, 2022.

Correspondence
Address correspondence to: Xin Yin, MD, PhD, Liver Cancer Institute, Zhongshan Hospital, Fudan University, 136 Yi Xue Yuan Road, Shanghai 200032, China. e-mail: yin.xin@zs-hospital.sh.cn.

CRediT Authorship Contributions

Feng Zhang (Conceptualization: Equal; Formal analysis: Lead; Methodology: Lead; Project administration: Lead; Writing – original draft: Lead; Writing – review & editing: Equal)

Keshu Hu (Methodology: Equal; Project administration: Equal; Writing – original draft: Equal)

Wenfeng Liu (Investigation: Lead; Methodology: Equal; Project administration: Equal)

Bing Quan (Methodology: Equal; Software: Lead; Validation: Lead)

Miao Li (Data curation: Lead; Formal analysis: Equal)

Shenxin Lu (Data curation: Equal; Formal analysis: Equal; Investigation: Equal)

Rongxin Chen (Conceptualization: Equal; Resources: Lead; Supervision: Equal)

Zhenggang Ren (Conceptualization: Equal; Supervision: Equal)

Xin Yin (Conceptualization: Lead; Data curation: Equal; Funding acquisition: Lead; Supervision: Lead; Validation: Equal; Writing – review & editing: Lead)

Conflicts of interest
The authors disclose no conflicts.

Funding
This work was supported by grants 81972889 and 81672331 from the National Natural Science Foundation of China, and by grant 2021-001 from the Exploratory Clinical Research Projects of National Clinical Research Center for Interventional Medicine.